A spectral analysis of the nonlinear Schrödinger equation in the co-exploding frame

S.J. Chapman [a,*], M. Kavousanakis [b], E.G. Charalampidis [c], I.G. Kevrekidis [d,e], P.G. Kevrekidis [f]

[a] *Mathematical Institute, University of Oxford, AWB, ROQ, Woodstock Road, Oxford OX2 6GG, United Kingdom*
[b] *School of Chemical Engineering, National Technical University of Athens, 15780, Athens, Greece*
[c] *Mathematics Department, California Polytechnic State University, San Luis Obispo, CA 93407-0403, USA*
[d] *Department of Chemical and Biomolecular Engineering, Johns Hopkins University, Baltimore, MD 21218, USA*
[e] *Department of Applied Mathematics and Statistics, Johns Hopkins University, Baltimore, MD 21218, USA*
[f] *Department of Mathematics and Statistics, University of Massachusetts, Amherst MA 01003-4515, USA*

ARTICLE INFO

ABSTRACT

The nonlinear Schrödinger model is a prototypical dispersive wave equation that features finite time blowup, either for supercritical exponents (for fixed dimension) or for supercritical dimensions (for fixed nonlinearity exponent). Upon identifying the self-similar solutions in the so-called "co-exploding frame", a dynamical systems analysis of its stability is natural, yet is complicated by the mixed Hamiltonian-dissipative character of the relevant frame. In the present work, we study the spectral picture of the relevant linearized problem. We examine the point spectrum of 3 eigenvalue pairs associated with translation, $U(1)$ and conformal invariances, as well as the continuous spectrum. We find that two eigenvalues become positive, yet are attributed to symmetries and are thus not associated with instabilities. In addition to a vanishing eigenvalue, 3 more are found to be negative and real, while the continuous spectrum is nearly vertical and on the left-half (spectral) plane. The eigenfunctions and eigenvalues are approximated both asymptotically and numerically, with good agreement between the two approaches. The non-Hamiltonian nature of the co-exploding system results in the 3 eigenvalue pairs failing to be equal-and-opposite by an exponentially small amount. A projection method is used to evaluate this small correction, and at the same time explains the subtle effects of finite boundaries and their role in the observed weak eigenvalue oscillations.

1. Introduction

One of the central dispersive nonlinear partial differential equations of relevance to a wide range of physical systems is the nonlinear Schrödinger (NLS) model [1–5]. Among the different research themes where the NLS plays a central role, one can mention the study of the electric field of light in nonlinear optical systems [6,7], as well as in plasmas [8], the realm of water waves and the evolution of their height, e.g., in deep water [9,10], as well as the condensate wavefunction for mean-field models of atomic Bose–Einstein condensates (BECs) [5,11,12]. The prototypical variants of the equation involve the self-focusing [4,13] and the self-defocusing nonlinearity [5], and the respective dynamics revolve around bright [14] and dark [15] solitons.

In the case of self-focusing (self-attractive) nonlinearity, and for sufficiently high dimension (for fixed nonlinearity) or for sufficiently strong nonlinearity (for fixed dimension), a key feature of the NLS model is the presence of collapse type phenomena, that have also been explored in numerous books [4,13,16], as well as reviews [17–19]. Indeed, the topic of finite time blow up of supercritical NLS solutions has been the objective of continued study both in the mathematical and in the physical literature; see, e.g., Refs. [20–24] (and also references therein) for only some recent examples. Importantly, the study of collapse is not only a mathematical idealization but rather has become accessible to physical experiments. In fact, on the one hand, there is the well-developed field of nonlinear optics, where not only the well-known, two-dimensional collapsing waveform of the Townes soliton has been observed [25] but also more

---

* Corresponding author.
E-mail address: chapman@maths.ox.ac.uk (S.J. Chapman).

elaborate themes have been touched upon including the collapse of optical vortices [26], the loss of phase information of collapsing filaments [27], and the manipulation of the medium to avert optical collapse [28]. On the other hand, a remarkable, very recent experimental development has been the emergence of 2 distinct works in the atomic physics realm of BECs, observing Townes solitons in the 2d setting [29,30]. Here, collapsing waveforms in higher dimensions had been experimentally identified earlier [31,32], and the ability to manipulate the nonlinearity [33] and the initial conditions [34] has continued to improve in recent times. In one of these recent works [29] the modulational instability was manipulated to produce (in a less controllable, yet experimentally observable) way such Townes waveforms. The authors of the second work [30] leveraged a reduction of a minority component in a two-component gas into a single-component one with *effectively attractive* interactions to produce a collapsing Townes waveform.

In many of the above mathematical works that study the dynamics of collapse, both in dispersive systems such as the NLS [4,13], but also even in dissipative systems such as reaction–diffusion ones [35], the emphasis is on identifying the solution in a frame where it becomes steady, namely a self-similar (or "co-exploding") one [36–40]. A similar approach is leveraged in dynamical systems and partial differential equations (PDEs) when exploring travelling waves which are identified as steady solutions in a so-called co-travelling frame. In such settings, a natural next step is to explore the spectral stability of the solutions in such a frame [41,42]. However, in the realm of the self-similar solutions, far fewer studies appear to be exploring the spectral properties of the wave in the co-exploding frame [43–45]. Indeed, in the context of NLS, the only earlier approach, to the best of our knowledge, towards spectrally exploring the collapse problem concerns the earlier work of some of the authors [45]. In a recent work, we revisited this topic, attempting to examine the self-focusing problem as a bifurcation one, identifying its effective normal form [46]. In the present study, we complement this approach by systematically examining the spectrum of the self-similarly collapsing solitary wave.

Upon setting up the relevant linearization problem in the self-similar frame (in Section 2), our starting point will consist of observations of the spectrum of the underlying Hamiltonian system before the bifurcation point (in Section 3). We will examine the relevant spectral picture when approaching the limit point where collapsing solutions emerge, and also we will explore the same picture for the *dissipative* system that results in the co-exploding frame past the critical point. The former reveals three eigenvalue pairs at the origin at the critical point (associated with translation, $U(1)$, and conformal invariances), and a key part of our analysis is tracking the behaviour of these pairs in the co-exploding frame past the critical point. In Section 4 we approximate each eigenvalue asymptotically, finding that the pairs fail to be equal-and-opposite by an exponentially small amount. Finally, we will synthesize the picture and its dynamical implications and offer some conclusions and future challenges in Section 5. The Appendices offer some additional insights, including about how a symmetry of the original frame can turn into an unstable eigendirection in a renormalized one, as well as about the role of the normal form obtained previously in [46] in connection with the eigenvalues identified herein.

2. Basic mathematical setup

Our model of interest will be the one-dimensional, general-nonlinearity-exponent variant of NLS in the form

$$\mathrm{i}\frac{\partial \psi}{\partial z} + \frac{\partial^2 \psi}{\partial x^2} + |\psi|^{2\sigma}\psi = 0. \tag{1}$$

Notice that here we have used the typical optics notation, where z is the evolution variable, representing the propagation distance [4]. This model has been studied extensively in [4,13] and it is well-known that in d-dimensions, the condition for its collapse is $\sigma d > 2$. The model is subcritical for $\sigma d < 2$, and the special case of $\sigma d = 2$ separates the two regimes. We opt to consider the $d = 1$ case for a number of practical reasons, including (a) the availability of an analytical solution for all values of σ, namely $\psi = \mathrm{e}^{\mathrm{i}z}(1 + \sigma)^{1/(2\sigma)}\,\mathrm{sech}\left[(2\sigma)^{1/2}(x - x_0)\right]$ and (b) the computational convenience of the relevant spectral calculations. As we will see below, the latter will be sensitively dependent on the domain size and its boundary conditions, and associated considerations will be even more delicate (and imposing a substantial additional computational overhead) in higher dimensions. Nevertheless, we expect the main features and techniques proposed herein to be directly reflected in such higher-dimensional settings, as will be evident in what follows.

The Hamiltonian associated with Eq. (1) is given by

$$H = \int_{-\infty}^{\infty}\left(\left|\frac{\partial \psi}{\partial x}\right|^2 - \frac{1}{\sigma + 1}|\psi|^{2\sigma + 2}\right)\mathrm{d}x. \tag{2}$$

The dynamical equations satisfy:

$$\mathrm{i}\frac{\partial \psi}{\partial z} = \frac{\delta H}{\delta \psi^*}, \qquad \mathrm{i}\frac{\partial \psi^*}{\partial z} = -\frac{\delta H}{\delta \psi}.$$

We require that H be finite.

In order to go to the co-exploding frame, we introduce the well-known [4,13] stretched variables, rescaling space by the length scale $L(z)$
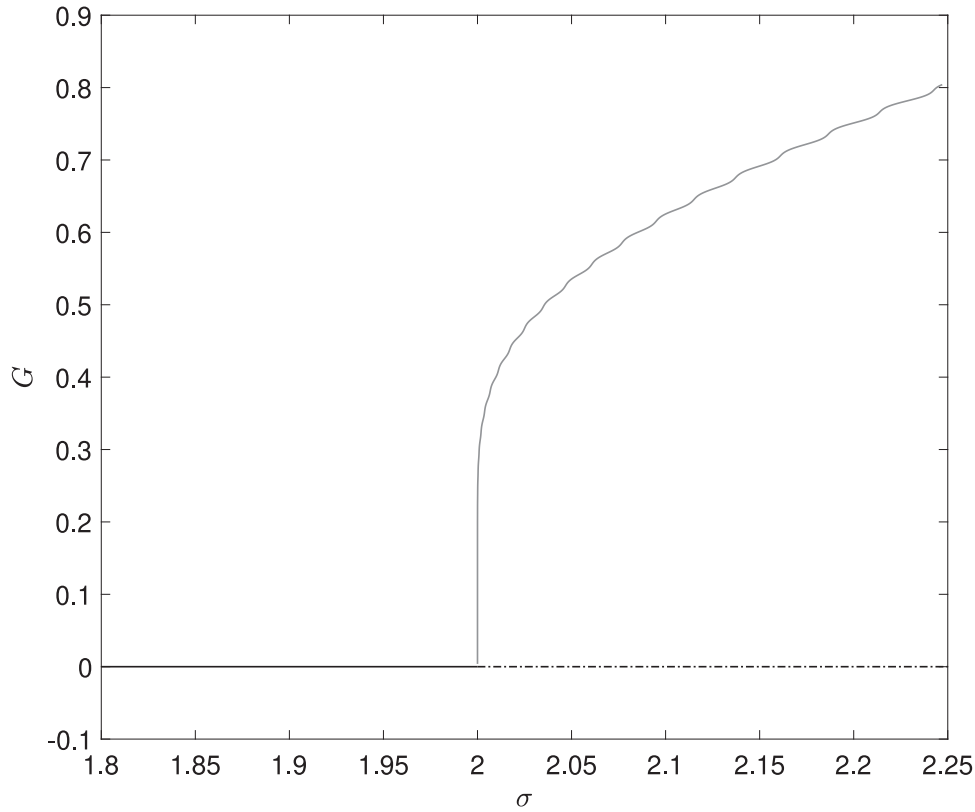
$$\xi = \frac{x}{L(z)}, \quad \tau = \int_0^z \frac{\mathrm{d}z'}{L^2(z')}, \quad \psi(x, z) = L^{-1/\sigma}u(\xi, \tau), \tag{3}$$

to give

$$\mathrm{i}\frac{\partial u}{\partial \tau} + \frac{\partial^2 u}{\partial \xi^2} + |u|^{2\sigma}u - \mathrm{i}\xi L L_z \frac{\partial u}{\partial \xi} - \frac{\mathrm{i}L L_z}{\sigma}u = 0, \tag{4}$$

and the corresponding rescaling of the Hamiltonian:

$$H = L^{-2/\sigma - 2}\int_{-\infty}^{\infty}\left(\left|\frac{\partial u}{\partial \xi}\right|^2 - \frac{1}{\sigma + 1}|u|^{2\sigma + 2}\right)\mathrm{d}x. \tag{5}$$

Fig. 1. Variation of blowup rate G as a function of σ, for domain size $K = 20$. The solitonic branch ($G = 0$) remains stable up to $\sigma = 2$ (black solid line) and becomes unstable for $\sigma > 2$ (black dash-dotted line). The stable collapsing branch ($G > 0$) is illustrated with solid grey line.

We factor out the frequency of our solution without loss of generality and assign the rate of width shrinkage/amplitude growth to be termed as G by setting

$$u(\xi, \tau) = \Phi(\xi, \tau)e^{i\tau}, \qquad G(\tau) = -LL_z = -\frac{L_\tau}{L}, \tag{6}$$

which reduce Eq. (4) into

$$i\frac{\partial \Phi}{\partial \tau} + \frac{\partial^2 \Phi}{\partial \xi^2} + |\Phi|^{2\sigma}\Phi - \Phi + \frac{iG}{\sigma}\Phi + iG\xi\frac{\partial \Phi}{\partial \xi} = 0. \tag{7}$$

In order to close the dynamics and determine the blow-up rate G we impose a pinning condition of the form [46]

$$\int_{-\infty}^{\infty} \mathrm{Re}(\Phi(\xi, \tau))T(\xi)\,\mathrm{d}\xi = C, \tag{8}$$

for some constant C and some (essentially arbitrary) "template function" T. Solitonic solutions correspond to $G = 0$, and exist for all $\sigma > 0$, but there is a bifurcation at $\sigma = 2$, with a branch of steady solutions with nontrivial $G > 0$ (i.e. self-similar blow-up solutions of (1)) appearing for $\sigma > 2$ [4,45,46]. The bifurcation diagram is shown in Fig. 1, and a typical example of the associated waveforms and the dynamics approaching them in Eq. (7) is shown in Fig. 2.

In [46] we showed that, when $\sigma - 2$ is small, G (asymptotically) satisfies the ODE

$$2c_0 G\frac{\mathrm{d}G}{\mathrm{d}\tau} = \frac{(\sigma - 2)}{2\sigma}b_0 G - A_1^2 \,\mathrm{sign}(G)\,e^{-\pi/|G|}, \tag{9}$$

where

$$c_0 = \frac{\sqrt{3}\,\pi^3}{512}, \qquad b_0 = \frac{\sqrt{3}\,\pi}{4}, \qquad A_1 = 12^{1/4}, \tag{10}$$

which can be thought of as the normal form associated with the bifurcation. We see in (9) a stable branch of equilibrium solutions $G > 0$ appearing for $\sigma > 2$. These results suggest the attractivity of the self-similar blow-up solutions, and hence predispose us towards their (effective) spectral stability.

It is particularly important for our considerations that follow to emphasize that the system (7) bears a rather unusual "mixed" character. Along the manifold of $G = 0$ (solitonic) solutions, the relevant model falls back on the original one, retaining its Hamiltonian structure. Nevertheless, for the genuinely self-similar solutions of $G \neq 0$, the system is no longer conservative in nature. Hence, we are dealing with a mixed Hamiltonian-dissipative system and the dissipativity for $G \neq 0$ should be mirrored in the spectrum of the
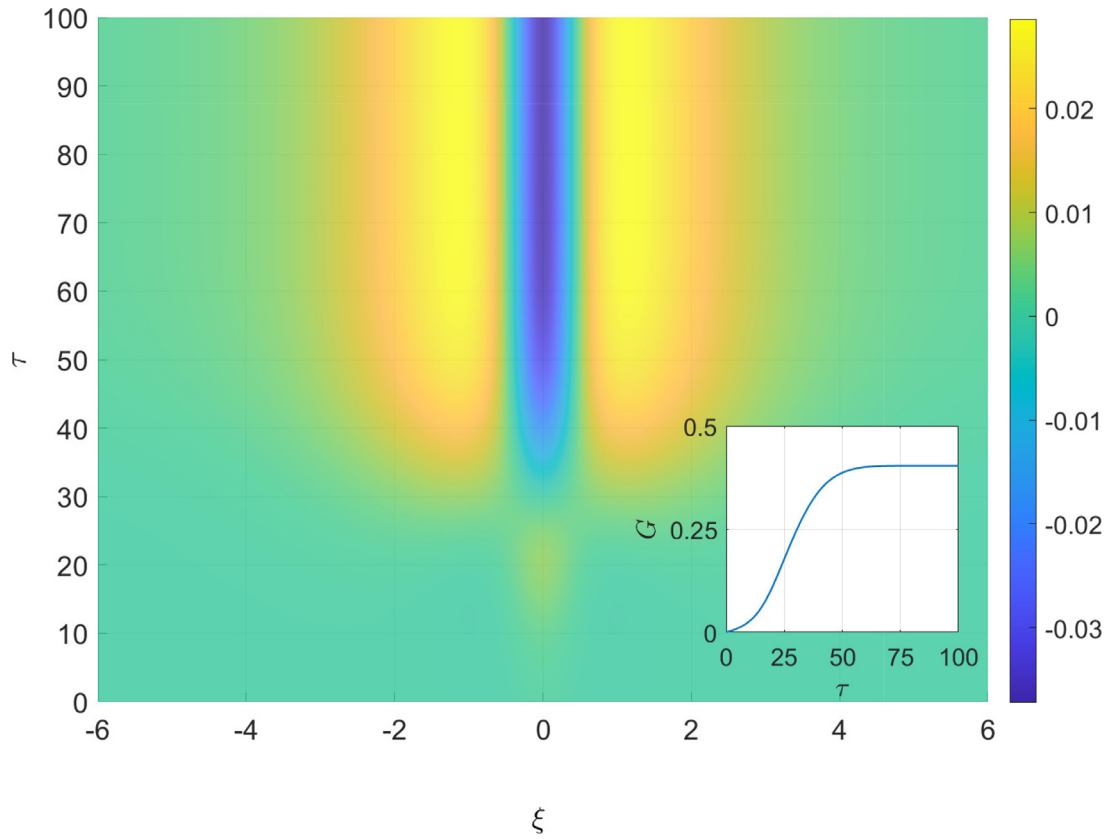
Fig. 2. Dynamics of $|\Phi(\xi, \tau)|^2 - |\Phi(\xi, 0)|^2$ in the co-exploding frame (rescaled NLS). The initial condition, $\Phi(\xi, 0)$ is the soliton solution for $\sigma = 2.019$. Upon perturbing σ to $\sigma = 2.02$, the co-exploding dynamics converges to a "steady-state" solution. The inset on the bottom right illustrates the evolution of the blowup rate, G, with the rescaled time, τ.

self-similar solutions. This is contrary to what is the case for the four-fold symmetric spectrum of the $G = 0$ solitons, for which if λ is an eigenvalue, so are $-\lambda$, λ^* and $-\lambda^*$.

We will find it convenient to perform an additional transformation by writing

$$\Phi(\xi, \tau) = V(\xi, \tau)e^{-iG(\tau)\xi^2/4} \tag{11}$$

to give

$$i\frac{\partial V}{\partial \tau} + \frac{G'\xi^2}{4}V + \frac{\partial^2 V}{\partial \xi^2} + |V|^{2\sigma}V - V - \frac{i(\sigma - 2)G}{2\sigma}V + \frac{G^2\xi^2}{4}V = 0, \tag{12}$$

where $G' = dG/d\tau$, since then (without loss of generality) the imaginary part of V is exponentially small in G [46]. Notice that above we have suppressed the dependence of G on the parameter σ.

Our principal aim is to consider the spectral stability of the steady-state solutions (with $G \neq 0$) in the co-exploding frame. These correspond to self-similar blowup solutions in the original frame. Such steady-state solutions denoted by Φ_s satisfy

$$\frac{d^2\Phi_s}{d\xi^2} + |\Phi_s|^{2\sigma}\Phi_s - \Phi_s + \frac{iG}{\sigma}\Phi_s + iG\xi\frac{d\Phi_s}{d\xi} = 0, \tag{13}$$

or equivalently

$$\frac{d^2V_s}{d\xi^2} + |V_s|^{2\sigma}V_s - V_s - \frac{i(\sigma - 2)G}{2\sigma}V_s + \frac{G^2\xi^2}{4}V_s = 0, \tag{14}$$

with G constant equal to $G(\sigma)$ illustrated in Fig. 1. We now linearize Eq. (7) about Φ_s by setting:

$$\Phi(\xi, \tau) = \Phi_s(\xi) + \epsilon\left(X(\xi)e^{\lambda\tau} + Y^*(\xi)e^{\lambda^*\tau}\right), \quad \epsilon \ll 1, \tag{15}$$

giving rise to the operator eigenvalue problem

$$i\lambda X = \left(-\frac{d^2}{d\xi^2} - (\sigma + 1)|\Phi_s|^{2\sigma} + 1 - \frac{iG}{\sigma} - iG\xi\frac{d}{d\xi}\right)X - \sigma|\Phi_s|^{2\sigma-2}\Phi_s^2 Y, \tag{16}$$

$$i\lambda Y = \sigma|\Phi_s|^{2\sigma-2}(\Phi_s^*)^2 X + \left(\frac{d^2}{d\xi^2} + (\sigma + 1)|\Phi_s|^{2\sigma} - 1 - \frac{iG}{\sigma} - iG\xi\frac{d}{d\xi}\right)Y. \tag{17}$$

Equivalently, for the stationary solution $V_s(\xi)$, we linearize in ϵ by writing

$$V(\xi, \tau) = V_s(\xi) + \epsilon \left(f(\xi)e^{\lambda \tau} + g^*(\xi)e^{\lambda^* \tau} \right) \tag{18}$$

which leads to

$$i\lambda f + \frac{d^2 f}{d\xi^2} + \sigma |V_s|^{2\sigma-2} V_s^2 g + (\sigma+1)|V_s|^{2\sigma} f - f - \frac{i(\sigma-2)G}{2\sigma} f + \frac{G^2 \xi^2}{4} f = 0, \tag{19}$$

$$-i\lambda g + \frac{d^2 g}{d\xi^2} + \sigma |V_s|^{2\sigma-2} (V_s^*)^2 f + (\sigma+1)|V_s|^{2\sigma} g - g + \frac{i(\sigma-2)G}{2\sigma} g + \frac{G^2 \xi^2}{4} g = 0. \tag{20}$$

To solve numerically we truncate the domain and solve on the finite domain $[-K, K]$, imposing the boundary conditions

$$\frac{\partial \Phi}{\partial \xi} = 0 \qquad \text{at } \xi = \pm K,$$

which correspond to

$$\frac{\partial V}{\partial \xi} = \pm \frac{iGKV}{2} \qquad \text{at } \xi = \pm K.$$

(The finiteness of the domain is what leads to the small oscillations in the bifurcation diagram Fig. 1, as explained in [46].) For the perturbation this gives, correspondingly,

$$\frac{\partial X}{\partial \xi} = \frac{\partial Y}{\partial \xi} = 0, \qquad \frac{\partial f}{\partial \xi} = \pm \frac{iGKf}{2}, \qquad \frac{\partial g}{\partial \xi} = \mp \frac{iGKg}{2} \qquad \text{on } \xi = \pm K.$$

Let us now try to explore, on the basis of the above principal setup, what we should expect to see in the linearization around a collapsing waveform.

3. Principal numerical results

The question of how the spectrum changes under the type of nontrivial scaling transformation discussed above requires particular attention. This topic was first addressed systematically, to the best of our knowledge, in a different class of systems, in the pioneering work of [43,44] who realized that such a transformation that rescales space and time may have profound implications within the renormalized frame as regards the interpretations of symmetries of the original frame. To explain this subtle point, we provide arguably the simplest possible example that we have been able to identify in Appendix A of the present manuscript. There, and in the cleaner/simpler setting of an autonomous ordinary differential equation, it can be seen that the symmetry of time translation of the original system leads to an "apparent instability" in the renormalized frame. This is because a shift in, e.g., the time of collapse in the original frame, due to the exponential nature of the transformation between the renormalized and the regular time, leads to an exponential deviation in the renormalized frame and hence an *apparent* instability.

The key take-home message from this example is that *symmetries of the original frame may no longer correspond to ones such in the renormalized frame*. The even more dire consequence is that *symmetries of the original frame may appear as instabilities in the renormalized one*. For example, differentiating Eq. (13) with respect to ξ gives

$$\frac{d^3 \Phi_s}{d\xi^3} + (\sigma+1)|\Phi_s|^{2\sigma} \frac{d\Phi_s}{d\xi} + \sigma |\Phi_s|^{2\sigma-2} \Phi_s^2 \frac{d\Phi_s^*}{d\xi} - \frac{d\Phi_s}{d\xi} + \frac{iG}{\sigma} \frac{d\Phi_s}{d\xi} + iG\xi \frac{d^2 \Phi_s}{d\xi^2} + iG \frac{d\Phi_s}{d\xi} = 0, \tag{21}$$

from which we observe that $X = d\Phi_s/d\xi$ and $Y = d\Phi_s^*/d\xi$ satisfy Eqs. (16)–(17) if we choose $\lambda = G$. The eigenvector is associated with the derivative, which is well-known to be the generator of translations. However, instead of this vector being associated with a neutral direction, it is now associated with an "apparently unstable" eigenmode (since $G > 0$). Nevertheless, that eigenmode is *not* a true instability in the original frame, even though it appears as one in the renormalized frame. Rather, it only involves spatial translation, i.e., a symmetry, and its suitable reinterpretation in this renormalized frame.

Armed with this important piece of understanding, let us now scrutinize the spectral picture in further detail. As is natural, we start with the subcritical case of $\sigma d < 2$. In this regime, only the solitary wave solution of $G = 0$ is present and hence it is the stability of this branch that we comment on first. In the integrable limit of $d = \sigma = 1$, it is well-known [47] that the spectrum of the linearization of the NLS soliton possesses two neutral directions, one associated with spatial translations, and one associated with the phase or gauge (U(1)) invariance. We already saw that the derivative $d\Phi_s/d\xi$ is connected to the translational eigenvector while the solution Φ_s itself is associated with the corresponding phase eigenvector. In each case, the generalized eigenvectors are known as well [47].

As we depart (parametrically in σ) from the integrable limit, an eigenvalue pair bifurcates from the band edge of the continuous spectrum which consists of the union of the intervals $i[1, \infty)$ and $-i[1, \infty)$ and tends (along the imaginary axis) towards the origin as $\sigma \to 2$. It is this eigenvalue pair that arrives at the origin of the spectral plane, precisely at $\sigma = 2$, instituting the conformal invariance of the model, i.e., the invariance with respect to rescaling that paves the way to collapse dynamics. The dependence of this eigenvalue on the parameter σ is shown in Fig. 3. Past the critical point, the relevant eigenvalue becomes real, giving rise to the dynamical instability of the soliton and the emergence of the collapsing branch of solutions. The spectra of the solitonic solution of $G = 0$ for σ below the critical point ($\sigma_c = 2$ for $d = 1$) and above the critical point are shown in Fig. 4.

As the bifurcation of the self-similarly focusing branch of solutions occurs [45,46], the natural question is what becomes of the spectrum and what are the corresponding dynamical implications of this spectral linearization picture. Recall that at the critical point, the "parent branch" of solitary waves has, in addition to the above mentioned continuous spectrum, 3 eigenvalue pairs at the origin. Hence, as this Hamiltonian system turns dissipative for $G > 0$, we have to determine the fate of the 6 eigenvalues stemming from the origin, and the associated continuous spectrum band. Notice that the 6 eigenvalues will *no longer* constitute pairs, except perhaps approximately, as the dissipativity of $G \neq 0$ destroys the Hamiltonian character and hence the eigenvalue pairing.
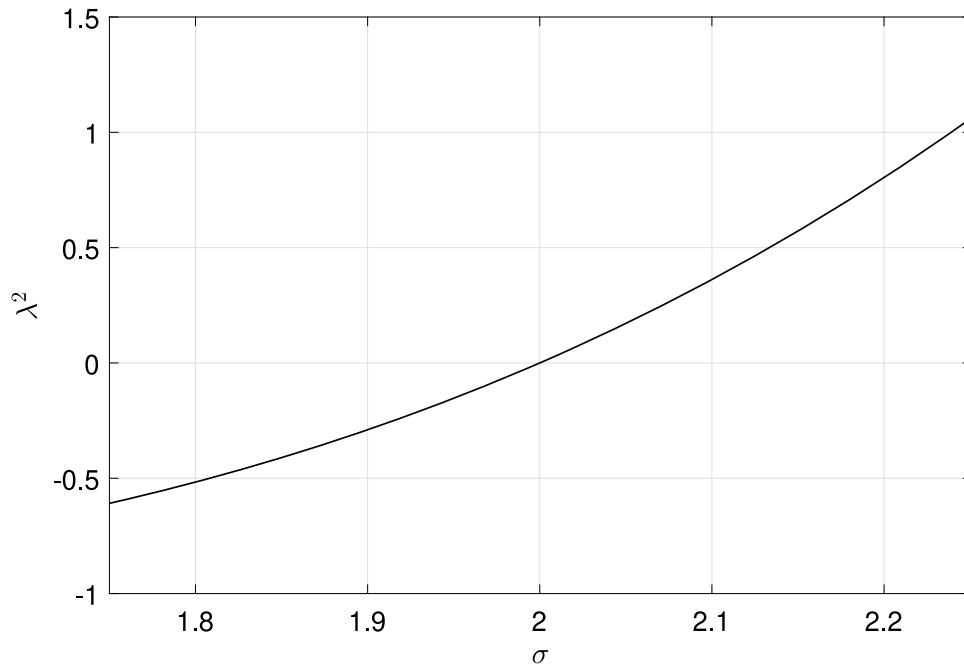
Fig. 3. Square of eigenvalue bifurcating from the band edge of the continuous spectrum, tending towards the origin as $\sigma \to 2$, and finally giving rise to real eigenvalues (one positive and one negative) past the critical point, $\sigma = 2$.
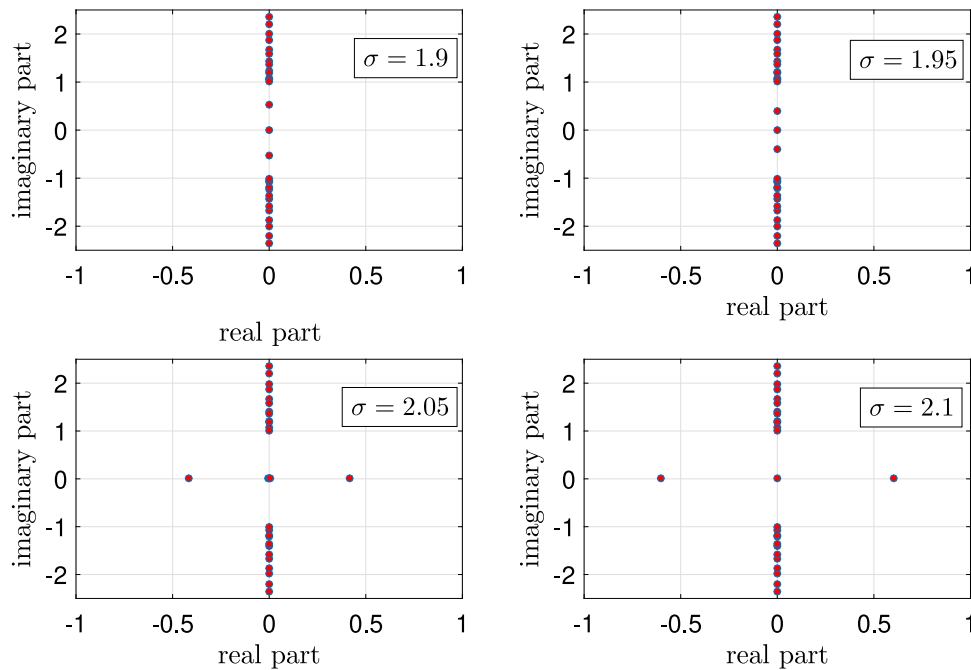

Fig. 4. Spectra of the numerically obtained soliton solution ($G = 0$) of the rescaled NLS equation with $K = 20$ and $\sigma = 1.9$, $\sigma = 1.95$, $\sigma = 2.05$ and $\sigma = 2.1$.

Having obtained the collapsing solutions with finite non-vanishing G as stationary ones (see the details in [46]), we are now ready to solve the corresponding spectral problem for the eigenvalues λ and eigenvectors (X, Y). Some typical examples of the spectral plane of the imaginary vs. the real part of the eigenvalues for specific choices of σ (and hence G, per Fig. 1) are shown in Fig. 5. The answer to this central question of our manuscript for the spectrum of the collapsing solution for supercritical values of σ and non-vanishing G in the co-exploding frame is given in Fig. 6. There we can see that, in fact, *only one* out of the 6 eigenvalues stays at the origin. Indeed, $X \propto \Phi_s$ remains an eigenvector with vanishing eigenvalue, as the rescaled model retains the original phase invariance. Nevertheless, as indicated above, the generalized eigenvector is no longer there (due to dissipativity) and, thus, the associated eigenvalue acquires a small negative value. We show in Section 4.2.5 that this eigenvalue is approximately

$$\lambda \sim -\frac{512 \, e^{-\pi/G}}{G^3 \pi^2},$$

with an eigenfunction exponentially close to that of the zero eigenvalue.
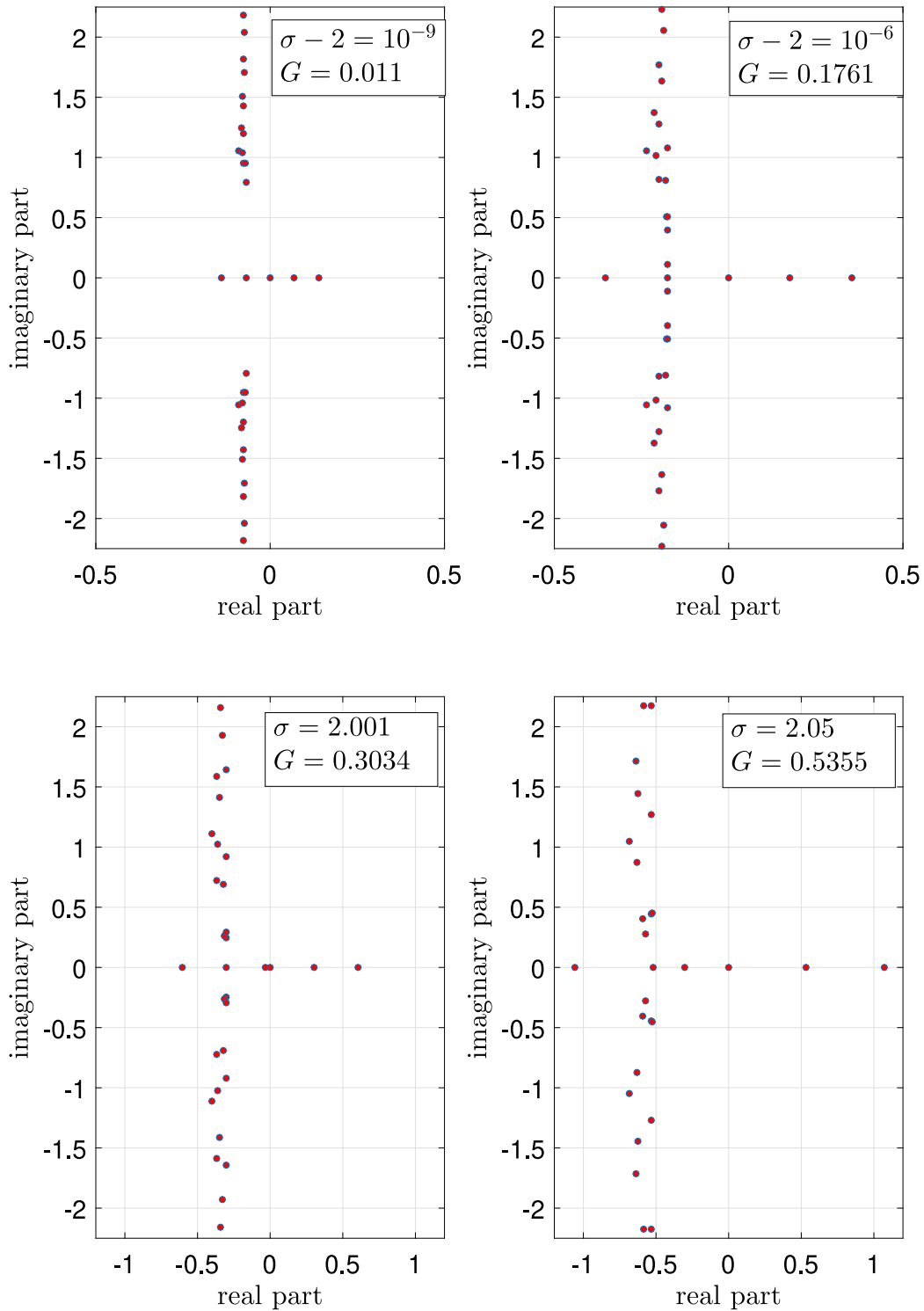
Fig. 5. Spectra of self-similar ($G > 0$) solutions obtained from the numerical solution of the rescaled NLS equation with $K = 20$ and σ values close to the critical value, $\sigma = 2$: $\sigma = 2 + 10^{-9}$ (top left panel) and $\sigma = 2 + 10^{-6}$ (top right panel), as well as $\sigma = 2.001$ (bottom left panel), $\sigma = 2.05$ (bottom right panel).

In addition, there are two pairs of eigenvalues that are only *nearly* symmetric. We find these to be at $\lambda \approx \pm 2G$ and $\lambda \approx \pm G$. All of these point spectrum eigenvalues are systematically captured in Fig. 6 to which we will return shortly. Moreover, there are two more observations in place regarding Fig. 5. One of the above 6 eigenvalues (and one of the ones shown in Fig. 6, as well), the eigenvalue at $\lambda \approx -G$, is hard to detect. This is because it almost coincides with a nearly vertical line of continuous spectrum with real part $\lambda_r = -G$, i.e., the continuous spectrum is approximately $\lambda = -G + is$ for arbitrary real s (see also Appendix B).

As we already discussed above, the pair at $\lambda \approx \pm G$ is associated with spatial translation. Indeed, the eigenvector $X = \mathrm{d}\Phi_s/\mathrm{d}\xi$, through the exact calculation above, yields an eigenvalue of $\lambda = G$ in the infinite domain. It can be discerned from Fig. 6, that this eigenvalue is no longer *exactly* at G on the finite domain but rather presents slight undulations in its dependence. Indeed, one of our
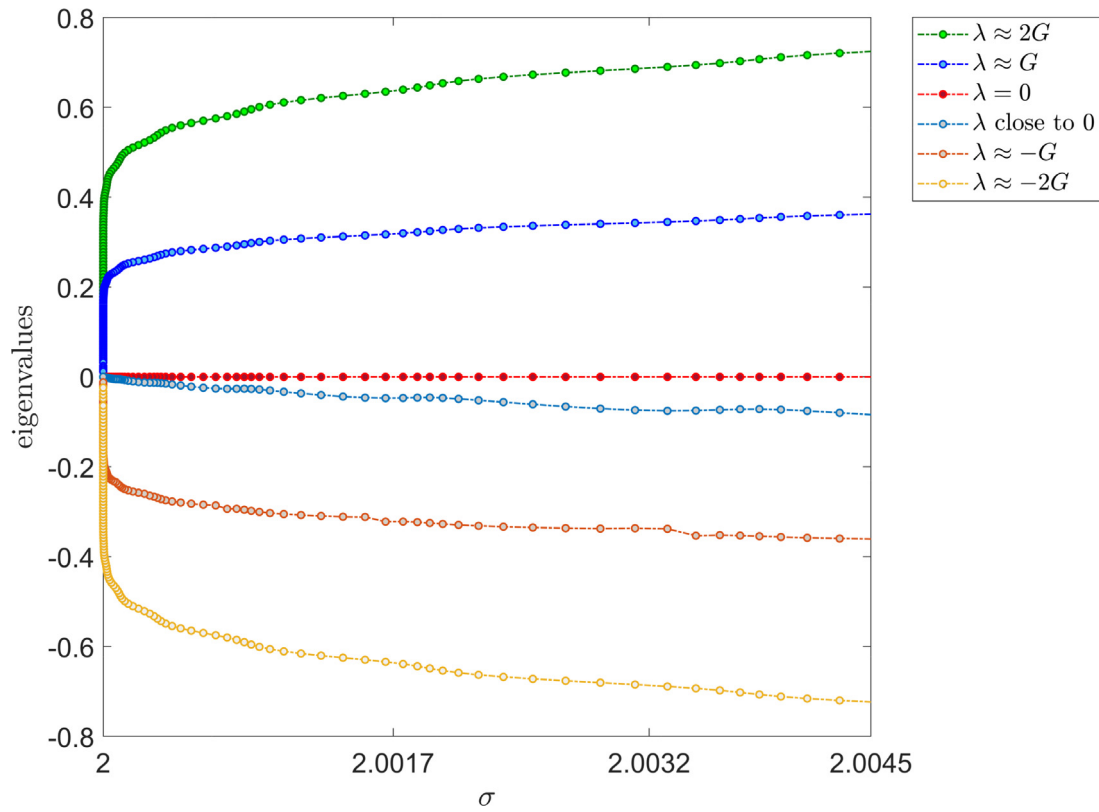
Fig. 6. Variation of the eigenvalues $\lambda \approx 2G$, $\lambda \approx G$, $\lambda = 0$, $\lambda \approx -G$, $\lambda \approx -2G$ and λ close to 0 with σ for the self-similar ($G > 0$) solutions as obtained from the numerical solution of the rescaled NLS equation with $K = 20$.

aims in the detailed calculations that follow will be to capture these finite-domain-induced undulatory corrections. On the other hand, the eigenvalue at $-G$ is no longer exact *even in the infinite domain*, due to the lack of symmetry, as induced by the dissipative terms $\propto G$ in our linearized equation for (X, Y) (or for (f, g)). The associated eigenvector is approximately

$$X = \frac{\mathrm{d}\Phi_s}{\mathrm{d}\xi} + \mathrm{i}G\xi\Phi_s$$

which satisfies the equation exactly but fails to satisfy the radiation condition. We show in Section 4.2.4 that this perturbs the eigenvalue by an exponentially small amount (in G), which is the source of the (more significant) undulations in this eigenvalue in Fig. 6.

In a very similar vein, the eigenvalue $\lambda = 2G$ is exact in the infinite domain limit, as can be verified by direct calculation, upon substituting the eigenvector

$$X = \mathrm{i}\Phi_s + G\left(\frac{\Phi_s}{\sigma} + \xi\frac{\mathrm{d}\Phi_s}{\mathrm{d}\xi}\right), \tag{22}$$

in the linearized equations. However, in this case too, the finite domain correction (to be also evaluated below) induces an undulatory dependence on top of the $\lambda = 2G$ leading order. Finally, the eigenvalue $\lambda = -2G$ is also no longer exact even for an infinite domain. The approximate eigenfunction is

$$X = \mathrm{i}\Phi_s - G\left(\frac{\Phi_s}{\sigma} + \xi\frac{\mathrm{d}\Phi_s}{\mathrm{d}\xi}\right) - \mathrm{i}G^2\xi^2\Phi_s,$$

which fails to satisfy the equation by an exponentially small residual, and also fails to satisfy the radiation condition at infinity, leading to an exponentially small correction to the eigenvalue. This summary then accounts for all the point spectrum eigenvalues.

It is relevant to add here two important observations. The first one concerns the dynamics of the collapsing solutions. On the one hand, we obtain that the relevant waveforms have two unstable eigendirections in the co-exploding frame. However, on the other hand, we have illustrated through our explicit calculations above (see also the pertinent Appendix A) that such eigendirections do not pertain to true instabilities, but rather to neutral directions of the original frame (spatial translations and rescalings of the original solution). Given the rescaling of space and time in the co-exploding frame, both of these actions move solutions exponentially far from other members of the family of such equivariant solutions, and thus appear as instabilities in the co-exploding frame, yet this is *not a true instability* in the original frame. Hence, in line with our above dynamical evolution results, we expect such collapsing solutions to be dynamically robust (modulo symmetries).

The second observation is related to the results for the spectrum given in the earlier work of [45]. There, only one of these positive eigenvalues was found and moreover the continuous spectrum had a wider apparent extent around $\lambda_r \approx -G$ (extending to values with more negative real part). The former of these features was because the calculation of [45] was done in the half-domain and hence,

e.g., spatial translations were a priori excluded from consideration. Furthermore, we believe that the observations of the continuous spectrum had to do with the discretization used in the latter case. Our refined numerics here suggest that the continuous spectrum progressively tends to the vertical line with $\lambda_r = -G$ (asymptotically for large imaginary part). Finally, we also note that the main features of the computed spectra show only slight changes by increasing the size of the computational domain (see Appendix C). Admittedly, in what follows we can only offer an asymptotic prediction for the part of the spectral band with sufficiently large imaginary part. For the part with small imaginary part, the situation is rather complex and constitutes a technical challenge for potential future studies. Nevertheless, we believe that we hereby offer a far more definitive perspective of both the point and the continuous spectrum, than was previously available.

In the analytical calculations that follow (and their comparison with the detailed numerical computations as regards the eigenvalue corrections), we will consider each of these eigenvalues one by one. We will split their dependence into a principal part (that we have effectively already discussed above), and a correction that stems either from the finiteness of the computational domain (in the case of $\lambda = G$ or $\lambda = 2G$) or from both the inexactness of the symmetry in the dissipative system *and* the radiation condition (in the case of the negative point spectrum eigenvalues). Since we work on a finite domain, this latter effect also appears though the boundary conditions.

We will develop a solvability-based approach to calculate the residual of each of these eigenvalues and will subsequently compare it to our systematic eigenvalue computations. Finally, we will corroborate our theoretical conclusion on the effective spectral stability (modulo the symmetries) of the collapsing solutions via direct numerical simulations in both the original and the co-exploding frame.

For the performance of numerical computations, we adopt a fourth-order central finite difference scheme for the approximation of spatial derivatives. Space, $\xi \in [-K, K]$ is uniformly discretized with step, $d\xi = 0.01$. Time integration (where needed) is performed utilizing MATLAB's ode23t ODE solver. Steady-state solutions are obtained through the iterative Newton–Raphson algorithm. Finally, the eigenvalue computations were performed by utilizing MATLAB's eig solver and corroborated further by using the contour-integral based FEAST eigenvalue solver [48] (and references therein). The spectral stability analysis results we obtained through the use of both eigenvalue solvers match precisely with each other.

4. Theoretical analysis approach

For our theoretical analysis, we work in terms of V_s, f and g. We first outline the general methodology, before we apply it to each eigenvalue of the discrete spectrum in turn.

For each of the point spectrum eigenvalues we have an asymptotic approximation to the eigenfunctions f_{reg} and g_{reg} and eigenvalue λ_{reg} which is accurate to all orders in G but misses exponentially small terms; here we aim to calculate those terms. [Notice that in what follows, for mathematical convenience, we will generally expand in powers of G, rather than the parameter σ.] Let us write $\lambda = \lambda_{\text{reg}} + \lambda_{\text{exp}}$. Then, Eqs. (19)–(20) give:

$$\mathrm{i}\lambda_{\text{reg}}f + \frac{\mathrm{d}^2 f}{\mathrm{d}\xi^2} + \sigma |V_s|^{2\sigma-2}V_s^2 g + (\sigma+1)|V_s|^{2\sigma}f - f - \frac{\mathrm{i}(\sigma-2)G}{2\sigma}f + \frac{G^2\xi^2}{4}f = -\mathrm{i}\lambda_{\text{exp}}f,$$

$$-\mathrm{i}\lambda_{\text{reg}}g + \frac{\mathrm{d}^2 g}{\mathrm{d}\xi^2} + \sigma |V_s|^{2\sigma-2}(V_s^*)^2 f + (\sigma+1)|V_s|^{2\sigma}g - g + \frac{\mathrm{i}(\sigma-2)G}{2\sigma}g + \frac{G^2\xi^2}{4}g = \mathrm{i}\lambda_{\text{exp}}g.$$

If we multiply by f_{reg} and g_{reg} respectively, add and integrate by parts, the left-hand side is

$$\int_{-K}^{K} \left(\mathrm{i}\lambda_{\text{reg}}f + \frac{\mathrm{d}^2 f}{\mathrm{d}\xi^2} + \sigma |V_s|^{2\sigma-2}V_s^2 g + (\sigma+1)|V_s|^{2\sigma}f - f - \frac{\mathrm{i}(\sigma-2)G}{2\sigma}f + \frac{G^2\xi^2}{4}f \right) f_{\text{reg}} \,\mathrm{d}\xi$$

$$+ \int_{-K}^{K} \left(-\mathrm{i}\lambda_{\text{reg}}g + \frac{\mathrm{d}^2 g}{\mathrm{d}\xi^2} + \sigma |V_s|^{2\sigma-2}(V_s^*)^2 f + (\sigma+1)|V_s|^{2\sigma}g - g + \frac{\mathrm{i}(\sigma-2)G}{2\sigma}g + \frac{G^2\xi^2}{4}g \right) g_{\text{reg}} \,\mathrm{d}\xi$$

$$= \int_{-K}^{K} \left(\mathrm{i}\lambda_{\text{reg}}f_{\text{reg}} + \frac{\mathrm{d}^2 f_{\text{reg}}}{\mathrm{d}\xi^2} + (\sigma+1)|V_s|^{2\sigma}f_{\text{reg}} - f_{\text{reg}} - \frac{\mathrm{i}(\sigma-2)G}{2\sigma}f_{\text{reg}} + \frac{G^2\xi^2}{4}f_{\text{reg}} \right) f \,\mathrm{d}\xi$$

$$\int_{-K}^{K} \left(-\mathrm{i}\lambda_{\text{reg}}g_{\text{reg}} + \frac{\mathrm{d}^2 g_{\text{reg}}}{\mathrm{d}\xi^2} + (\sigma+1)|V_s|^{2\sigma}g_{\text{reg}} - g_{\text{reg}} + \frac{\mathrm{i}(\sigma-2)G}{2\sigma}g_{\text{reg}} + \frac{G^2\xi^2}{4}g_{\text{reg}} \right) g \,\mathrm{d}\xi$$

$$+ \int_{-K}^{K} \sigma |V_s|^{2\sigma-2}V_s^2 \, gf_{\text{reg}} + \sigma |V_s|^{2\sigma-2}(V_s^*)^2 fg_{\text{reg}} \,\mathrm{d}\xi + \left[f_{\text{reg}}\frac{\mathrm{d}f}{\mathrm{d}\xi} - f\frac{\mathrm{d}f_{\text{reg}}}{\mathrm{d}\xi} + g_{\text{reg}}\frac{\mathrm{d}g}{\mathrm{d}\xi} - g\frac{\mathrm{d}g_{\text{reg}}}{\mathrm{d}\xi} \right]_{-K}^{K}$$

$$= \int_{-K}^{K} R_{\mathrm{f}}f + R_{\mathrm{g}}g + \sigma |V_s|^{2\sigma-2}(g_{\text{reg}}f - f_{\text{reg}}g)((V_s^*)^2 - V_s^2) \,\mathrm{d}\xi$$

$$+ \left[f_{\text{reg}}\frac{\mathrm{d}f}{\mathrm{d}\xi} - f\frac{\mathrm{d}f_{\text{reg}}}{\mathrm{d}\xi} + g_{\text{reg}}\frac{\mathrm{d}g}{\mathrm{d}\xi} - g\frac{\mathrm{d}g_{\text{reg}}}{\mathrm{d}\xi} \right]_{-K}^{K},$$

where

$$R_{\mathrm{f}} = \mathrm{i}\lambda_{\text{reg}}f_{\text{reg}} + \frac{\mathrm{d}^2 f_{\text{reg}}}{\mathrm{d}\xi^2} + (\sigma+1)|V_s|^{2\sigma}f_{\text{reg}} + \sigma |V_s|^{2\sigma-2}V_s^2 g_{\text{reg}} - f_{\text{reg}} - \frac{\mathrm{i}(\sigma-2)G}{2\sigma}f_{\text{reg}} + \frac{G^2\xi^2}{4}f_{\text{reg}},$$

$$R_{\mathrm{g}} = -\mathrm{i}\lambda_{\text{reg}}g_{\text{reg}} + \frac{\mathrm{d}^2 g_{\text{reg}}}{\mathrm{d}\xi^2} + (\sigma+1)|V_s|^{2\sigma}g_{\text{reg}} + \sigma |V_s|^{2\sigma-2}(V_s^*)^2 f_{\text{reg}} - g_{\text{reg}} + \frac{\mathrm{i}(\sigma-2)G}{2\sigma}g_{\text{reg}} + \frac{G^2\xi^2}{4}g_{\text{reg}},$$

are the exponentially small residuals from the regular asymptotic expansion. Since the imaginary part of V_s is exponentially small, and f_{reg} and g_{reg} are exponentially close to f and g, the term $(g_{\text{reg}}f - f_{\text{reg}}g)((V_s^*)^2 - V_s^2)$ is doubly exponentially small and can be neglected.

Then, evaluating also the right-hand side,

$$\int_{-K}^{K} (R_f f + R_g g)\, d\xi + \left[f_{\text{reg}} \frac{df}{d\xi} - f \frac{df_{\text{reg}}}{d\xi} + g_{\text{reg}} \frac{dg}{d\xi} - g \frac{dg_{\text{reg}}}{d\xi} \right]_{-K}^{K} \sim i\lambda_{\text{exp}} \int_{-K}^{K} (g_{\text{reg}} g - f_{\text{reg}} f)\, d\xi. \tag{23}$$

Since R_f, R_g and λ_{exp} are already exponentially small, we can use f_{reg}, g_{reg} in place of f and g except in the boundary terms, introducing only double-exponentially-small errors. Thus, to exponential accuracy,

$$\int_{-K}^{K} (R_f f_{\text{reg}} + R_g g_{\text{reg}})\, d\xi + \left[f_{\text{reg}} \frac{df}{d\xi} - f \frac{df_{\text{reg}}}{d\xi} + g_{\text{reg}} \frac{dg}{d\xi} - g \frac{dg_{\text{reg}}}{d\xi} \right]_{-K}^{K} \sim i\lambda_{\text{exp}} \int_{-K}^{K} (g_{\text{reg}}^2 - f_{\text{reg}}^2)\, d\xi. \tag{24}$$

This is the equation which determines the exponentially small correction to the eigenvalue λ_{exp}. To find the boundary terms we need to examine the far field more carefully, which we do in the next subsection. We believe that this decomposition (and identification) of exponentially small terms and of the contribution of boundary-induced reflections is relevant for a theoretical understanding of numerical observations of earlier computational works such as [45]. At the same time, the relevant asymptotic approach may also be of interest for other problems of this broad class of nonlinear partial differential equations.

4.1. Boundary condition on a finite domain

In this section we determine the boundary contribution to (24) by examining the far field, assuming that K is large. We will see that in the limit $K \to \infty$ the approximate eigenfunctions corresponding to eigenvalues $\lambda_{\text{reg}} > -G$ satisfy the radiation condition, while those corresponding to eigenvalues $\lambda_{\text{reg}} \leq -G$ do not.

Consider first f. We write $f = f_{\text{reg}} + f_b$, where f_b is the correction due to the fact that f_{reg} does not satisfy the boundary conditions. Note that in the far field both f_{reg} and f_b are exponentially small. Then, following the earlier work of [46], we have with $\rho = G\xi$,

$$f_{\text{reg}} = A_{\text{reg}}^{\text{f}} e^{i\phi_2/G} + B_{\text{reg}}^{\text{f}} e^{-i\phi_2/G}, \qquad f_b = A e^{i\phi_2/G} + B e^{-i\phi_2/G}, \tag{25}$$

where

$$\phi_2' = \sqrt{\frac{\rho^2}{4} - 1}, \qquad i\lambda_1 A + 2i\phi_2' A' + i\phi_2'' A = iGA'', \qquad i\lambda_1 B - 2i\phi_2' B' - i\phi_2'' B = iGB'', \tag{26}$$

and $\lambda_{\text{reg}} = \lambda_1 G$. Note that $A_{\text{reg}}^{\text{f}}$ and $B_{\text{reg}}^{\text{f}}$ are given, but A and B need to be determined. Expanding

$$A = \sum_{n=0}^{\infty} A_n(\rho)(iG)^n, \qquad B = \sum_{n=0}^{\infty} B_n(\rho)(-iG)^n, \tag{27}$$

substituting into Eq. (26), and equating coefficients of powers of G gives at leading order

$$\frac{A_0'}{A_0} = -\frac{(\phi_2'' + \lambda_1)}{2\phi_2'}, \qquad \frac{B_0'}{B_0} = -\frac{(\phi_2'' - \lambda_1)}{2\phi_2'},$$

so that

$$A_0 = \frac{a_{\text{f}}}{(\rho^2 - 4)^{1/4}} \left(\frac{\rho - \sqrt{\rho^2 - 4}}{\rho + \sqrt{\rho^2 - 4}} \right)^{\lambda_1/2}, \qquad B_0 = \frac{b_{\text{f}}}{(\rho^2 - 4)^{1/4}} \left(\frac{\rho + \sqrt{\rho^2 - 4}}{\rho - \sqrt{\rho^2 - 4}} \right)^{\lambda_1/2},$$

for some constants a_{f} and b_{f}. At the next order

$$\lambda_1 A_1 + 2\phi_2' A_1' + \phi_2'' A_1 = A_0'', \qquad -\lambda_1 B_1 + 2\phi_2' B_1' + \phi_2'' B_1 = B_0''.$$

Substituting for ϕ_2, A_0 and B_0, and solving gives

$$A_1 = \frac{a_{\text{f}}}{(\rho^2 - 4)^{1/4}} \left(\frac{\rho - \sqrt{\rho^2 - 4}}{\rho + \sqrt{\rho^2 - 4}} \right)^{\lambda_1/2} \frac{(24(2\lambda_1^2 - 1)\rho + (1 - 12\lambda_1^2)\rho^3 - 48\lambda_1\sqrt{\rho^2 - 4})}{48(\rho^2 - 4)^{3/2}},$$

$$B_1 = \frac{b_{\text{f}}}{(\rho^2 - 4)^{1/4}} \left(\frac{\rho + \sqrt{\rho^2 - 4}}{\rho - \sqrt{\rho^2 - 4}} \right)^{\lambda_1/2} \frac{(24(2\lambda_1^2 - 1)\rho + (1 - 12\lambda_1^2)\rho^3 + 48\lambda_1\sqrt{\rho^2 - 4})}{48(\rho^2 - 4)^{3/2}},$$

where we fix the constants of integration by requiring that $A \leftrightarrow B$ as we circle the branch point $\rho = 2$. Continuing in this way, we find that

$$A \sim a_{\text{f}} \rho^{-1/2 - \lambda_1} (1 + iG\mu_1 - \mu_2 G^2 + \cdots), \tag{28}$$

$$B \sim b_{\text{f}} \rho^{-1/2 + \lambda_1} (1 - iG\mu_1 + \mu_2 G^2 + \cdots), \tag{29}$$

as $\rho \to \infty$, where

$$\mu_1 = \frac{(1 - 12\lambda_1^2)}{48}, \qquad \mu_2 = \frac{\lambda_1(1 - 4\lambda_1^2)}{48}.$$

A similar asymptotic behaviour must hold for $A_{\text{reg}}^{\text{f}}$, $B_{\text{reg}}^{\text{f}}$, so that

$$A_{\text{reg}}^{\text{f}} \sim a_{\text{reg}}^{\text{f}} \rho^{-1/2 - \lambda_1} (1 + iG\mu_1 - \mu_2 G^2 + \cdots), \tag{30}$$

$$B^{\mathrm{f}}_{\mathrm{reg}} \sim b^{\mathrm{f}}_{\mathrm{reg}} \rho^{-1/2+\lambda_1}(1 - \mathrm{i}G\mu_1 + \mu_2 G^2 + \cdots) \tag{31}$$

as $\rho \to \infty$. As we approach the turning point $\rho = 2$,

$$A \sim \frac{a_{\mathrm{f}}}{(4(\rho - 2))^{1/4}}, \quad B \sim \frac{b_{\mathrm{f}}}{(4(\rho - 2))^{1/4}}.$$

Matching with the turning point region gives

$$a_{\mathrm{f}}\mathrm{i} = b_{\mathrm{f}},$$

which ensures that the extra contribution due to the reflection back from the boundary is exponentially small in the near field.

The boundary condition gives

$$\mathrm{i}\phi_2'(A + A^{\mathrm{f}}_{\mathrm{reg}})\mathrm{e}^{\mathrm{i}\phi_2/G} - \mathrm{i}\phi_2'(B + B^{\mathrm{f}}_{\mathrm{reg}})\mathrm{e}^{-\mathrm{i}\phi_2/G} + G(A' + A^{\mathrm{f}}_{\mathrm{reg}}{}')\mathrm{e}^{\mathrm{i}\phi_2/G} + G(B' + B^{\mathrm{f}}_{\mathrm{reg}}{}')\mathrm{e}^{-\mathrm{i}\phi_2/G}$$

$$= \frac{\mathrm{i}KG}{2}\left((A + A^{\mathrm{f}}_{\mathrm{reg}})\mathrm{e}^{\mathrm{i}\phi_2/G} + (B + B^{\mathrm{f}}_{\mathrm{reg}})\mathrm{e}^{-\mathrm{i}\phi_2/G}\right).$$

Eqs. (28)–(29) show that $A' = O(A/K)$ for large K, so that the term AK dominates A' by a factor of K^2. Neglecting the third and fourth terms on the left-hand side gives

$$\left(\phi_2' - \frac{KG}{2}\right)(A + A^{\mathrm{f}}_{\mathrm{reg}})\mathrm{e}^{\mathrm{i}\phi_2/G} = \left(\phi_2' + \frac{KG}{2}\right)(B + B^{\mathrm{f}}_{\mathrm{reg}})\mathrm{e}^{-\mathrm{i}\phi_2/G},$$

so that

$$\mathrm{e}^{2\mathrm{i}\phi_2/G}\frac{\sqrt{(KG)^2 - 4} - KG}{\sqrt{(KG)^2 - 4} + KG} = \frac{B + B^{\mathrm{f}}_{\mathrm{reg}}}{A + A^{\mathrm{f}}_{\mathrm{reg}}}.$$

We now assume that KG is large so that we can use the asymptotic behaviour of Eqs. (28)–(31) to evaluate the right-hand side, giving

$$\frac{\mathrm{i}a_{\mathrm{f}} + b^{\mathrm{f}}_{\mathrm{reg}}}{a_{\mathrm{f}} + a^{\mathrm{f}}_{\mathrm{reg}}} \sim -\frac{\mathrm{e}^{2\mathrm{i}\phi_2(KG)/G}}{(KG)^{2+2\lambda_1}}\left(\frac{1 + \mathrm{i}G\mu_1 - \mu_2 G^2 + \cdots}{1 - \mathrm{i}G\mu_1 + \mu_2 G^2 + \cdots}\right) = -S,$$

say. Then

$$a_{\mathrm{f}} \sim -\frac{b^{\mathrm{f}}_{\mathrm{reg}} + a^{\mathrm{f}}_{\mathrm{reg}}S}{\mathrm{i} + S}, \qquad b_{\mathrm{f}} \sim -\mathrm{i}\frac{b^{\mathrm{f}}_{\mathrm{reg}} + a^{\mathrm{f}}_{\mathrm{reg}}S}{\mathrm{i} + S}. \tag{32}$$

As $KG \to \infty$ the behaviour of S (and therefore a_{f} and b_{f}) crucially depends on whether λ_1 is greater or less than -1. For $\lambda_1 > -1$, $S \to 0$ as $KG \to \infty$ and

$$a_{\mathrm{f}} \sim \mathrm{i}b^{\mathrm{f}}_{\mathrm{reg}}, \qquad b_{\mathrm{f}} \sim -b^{\mathrm{f}}_{\mathrm{reg}}. \tag{33}$$

We will see that f_{reg} is such that $b^{\mathrm{f}}_{\mathrm{reg}} \to 0$ as $KG \to \infty$, so that the eigenfunctions corresponding to positive eigenvalues exactly satisfy the boundary condition (i.e. satisfy the radiation condition) in that limit. On the other hand, for $\lambda_1 < -1$, $S \to \infty$ as $KG \to \infty$ and

$$a_{\mathrm{f}} \sim -a^{\mathrm{f}}_{\mathrm{reg}}, \qquad b_{\mathrm{f}} \sim -\mathrm{i}a^{\mathrm{f}}_{\mathrm{reg}}. \tag{34}$$

Now $a^{\mathrm{f}}_{\mathrm{reg}}$ is finite even as $KG \to \infty$ so that the eigenfunctions corresponding to $\lambda_1 < -1$ fail to satisfy the boundary condition even in the limit $KG \to \infty$ (this is true for $\lambda_1 = -1$ also).

Now, for large KG, we can evaluate the boundary terms in Eq. (24) as

$$f_{\mathrm{reg}}\frac{\mathrm{d}f}{\mathrm{d}\xi} - f\frac{\mathrm{d}f_{\mathrm{reg}}}{\mathrm{d}\xi}\bigg|_{\rho=KG} = f_{\mathrm{reg}}\frac{\mathrm{d}f_b}{\mathrm{d}\xi} - f_b\frac{\mathrm{d}f_{\mathrm{reg}}}{\mathrm{d}\xi}\bigg|_{\rho=KG}$$

$$\sim G\left(A^{\mathrm{f}}_{\mathrm{reg}}\mathrm{e}^{\mathrm{i}\phi_2/G} + B^{\mathrm{f}}_{\mathrm{reg}}\mathrm{e}^{-\mathrm{i}\phi_2/G}\right)\left(\frac{\mathrm{i}\phi_2'}{G}\left(A\mathrm{e}^{\mathrm{i}\phi_2/G} - B\mathrm{e}^{-\mathrm{i}\phi_2/G}\right) + A'\mathrm{e}^{\mathrm{i}\phi_2/G} + B'\mathrm{e}^{-\mathrm{i}\phi_2/G}\right)$$

$$- G\left(A\mathrm{e}^{\mathrm{i}\phi_2/G} + B\mathrm{e}^{-\mathrm{i}\phi_2/G}\right)\left(\frac{\mathrm{i}\phi_2'}{G}\left(A^{\mathrm{f}}_{\mathrm{reg}}\mathrm{e}^{\mathrm{i}\phi_2/G} - B^{\mathrm{f}}_{\mathrm{reg}}\mathrm{e}^{-\mathrm{i}\phi_2/G}\right) + A^{\mathrm{f}}_{\mathrm{reg}}{}'\mathrm{e}^{\mathrm{i}\phi_2/G} + B^{\mathrm{f}}_{\mathrm{reg}}{}'\mathrm{e}^{-\mathrm{i}\phi_2/G}\right)$$

$$\sim -2\mathrm{i}\phi_2'(A^{\mathrm{f}}_{\mathrm{reg}}B - B^{\mathrm{f}}_{\mathrm{reg}}A)$$

$$\sim -\mathrm{i}(a^{\mathrm{f}}_{\mathrm{reg}}(1 + \mathrm{i}\mu_1 G + \cdots)b_{\mathrm{f}}(1 - \mathrm{i}\mu_1 G + \cdots) - b^{\mathrm{f}}_{\mathrm{reg}}(1 - \mathrm{i}\mu G + \cdots)a_{\mathrm{f}}(1 + \mathrm{i}\mu G + \cdots))$$

$$= -\mathrm{i}(a^{\mathrm{f}}_{\mathrm{reg}}b_{\mathrm{f}} - b^{\mathrm{f}}_{\mathrm{reg}}a_{\mathrm{f}})\left(1 - (\mathrm{i}\mu_1 G - \mu_2 G^2 + \cdots)^2\right).$$

A similar calculation on g shows that, when λ_1 is real,

$$g_{\mathrm{reg}}\frac{\mathrm{d}g}{\mathrm{d}\xi} - g\frac{\mathrm{d}g_{\mathrm{reg}}}{\mathrm{d}\xi}\bigg|_{\rho=KG} \sim -\mathrm{i}(a^{\mathrm{g}}_{\mathrm{reg}}b_{\mathrm{g}} - b^{\mathrm{g}}_{\mathrm{reg}}a_{\mathrm{g}})\left(1 - (-\mathrm{i}\mu_1 G - \mu_2 G^2 + \cdots)^2\right),$$

where

$$a_{\mathrm{g}} = \mathrm{i}\frac{a^{\mathrm{g}}_{\mathrm{reg}} + b^{\mathrm{g}}_{\mathrm{reg}}S^*}{-\mathrm{i} + S^*}, \qquad b_{\mathrm{g}} = -\frac{a^{\mathrm{g}}_{\mathrm{reg}} + b^{\mathrm{g}}_{\mathrm{reg}}S^*}{-\mathrm{i} + S^*},$$

so that

$$a_g \sim -a_{reg}^g, \qquad\qquad b_g \sim -i a_{reg}^g, \qquad\qquad \lambda_1 > -1, \tag{35}$$

$$a_g \sim i b_{reg}^g, \qquad\qquad b_g \sim -b_{reg}^g, \qquad\qquad \lambda_1 < -1. \tag{36}$$

A similar calculation of the boundary layer at $-K$ gives, finally,

$$
\left[f_{reg}\frac{df}{d\xi} - f\frac{df_{reg}}{d\xi} + g_{reg}\frac{dg}{d\xi} - g\frac{dg_{reg}}{d\xi} \right]_{-K}^{K} \sim
$$
$$
\begin{cases}
2ib_{reg}^f(a_{reg}^f + ib_{reg}^f)\left(1 - (i\mu_1 G - \mu_2 G^2 + \cdots)^2\right) & \\
\quad - 2ia_{reg}^g(-ia_{reg}^g + b_{reg}^g)\left(1 - (-i\mu_1 G - \mu_2 G^2 + \cdots)^2\right) & \text{if } \lambda_1 > -1, \\
\quad - 2ia_{reg}^f(-ia_{reg}^f + b_{reg}^f)\left(1 - (i\mu_1 G - \mu_2 G^2 + \cdots)^2\right) & \\
\quad + 2ib_{reg}^g(a_{reg}^g + ib_{reg}^g)\left(1 - (-i\mu_1 G - \mu_2 G^2 + \cdots)^2\right) & \text{if } \lambda_1 < -1.
\end{cases}
\tag{37}
$$

We will see that $a_{reg}^g = \left(b_{reg}^f\right)^*$ and $b_{reg}^g = \left(a_{reg}^f\right)^*$ so that the right-hand side is real.

4.2. Eigenvalues

We now apply the general methodology to each of the eigenvalues in turn. Since the approximate eigenfunctions f_{reg} and g_{reg} are given in terms of the steady state solution V_s, to identify the coefficients a_{reg}^f, a_{reg}^g, b_{reg}^f and b_{reg}^g that appear in the boundary terms, it is useful to recall the behaviour of V_s in the far field, which was determined in [46]. There we found that

$$V_s \sim \alpha e^{i\phi_2/G}\sum_{n=0}^{\infty} A_n(\rho)(iG)^n + \beta e^{-i\phi_2/G}\sum_{n=0}^{\infty} A_n(\rho)(-iG)^n, \qquad A_0(\rho) = \frac{2^{1/2}a_0}{(\rho^2 - 4)^{1/2}}, \tag{38}$$

where

$$a_0 = 12^{1/4},$$
$$\alpha = \frac{e^{i\pi/4}e^{-\pi/2G}}{1 - i\nu e^{2i\phi_2(KG)/G}} = e^{i\pi/4}e^{-\pi/2G} + \frac{i\nu e^{2i\phi_2(KG)/G}e^{i\pi/4}e^{-\pi/2G}}{1 - i\nu e^{2i\phi_2(KG)/G}},$$
$$\beta = -\nu\alpha e^{2i\phi_2(KG)/G} = -\frac{\nu e^{2i\phi_2(KG)/G}e^{i\pi/4}e^{-\pi/2G}}{1 - i\nu e^{2i\phi_2(KG)/G}},$$
$$\nu \sim \frac{KG - \sqrt{(KG)^2 - 4}}{KG + \sqrt{(KG)^2 - 4}} \sim \frac{1}{(KG)^2}.$$

4.2.1. The eigenvalue $\lambda_{reg} = 2G$

In terms of f and g the approximate eigenfunctions are

$$f_{reg} = iV_s + G\left(\frac{V_s}{\sigma} + \xi\frac{dV_s}{d\xi} - \frac{iG\xi^2 V_s}{2}\right), \quad g_{reg} = -iV_s^* + G\left(\frac{V_s^*}{\sigma} + \xi\frac{dV_s^*}{d\xi} + \frac{iG\xi^2 V_s^*}{2}\right). \tag{39}$$

These satisfy the equations exactly so that $R_f = R_g = 0$. The perturbation to the eigenvalue arises solely because of the finiteness of the domain, since f_{reg} and g_{reg} do not satisfy the boundary conditions. From the known expansion, Eq. (38) of the steady state solution, we need to identify the amplitude coefficients a_{reg}^f, b_{reg}^f in the WKB expansion [cf. Eqs. (25)–(27)]. The easiest way to do this is to compare the two representations of f_{reg} and g_{reg} as $\rho \to \infty$. Comparing Eqs. (38)–(39) with Eqs. (30)–(31) as $\rho \to \infty$ gives

$$a_{reg}^f\left(1 - i\frac{47G}{48}\right) \sim -i\sqrt{2}a_0\alpha\left(1 - i\frac{95G}{48} + \cdots\right),$$
$$b_{reg}^f\left(1 + i\frac{47G}{48}\right) \sim -i\sqrt{2}a_0\beta\left(1 - i\frac{G}{48} + \cdots\right),$$

since

$$\mu_1 = \frac{(1 - 12\lambda_1^2)}{48} = -\frac{47}{48}.$$

Thus,

$$a_{reg}^f \sim -i\sqrt{2}a_0\alpha\,(1 - iG), \qquad b_{reg}^f \sim -i\sqrt{2}a_0\beta\,(1 - iG), \qquad a_{reg}^g \sim \left(b_{reg}^f\right)^*, \qquad b_{reg}^g \sim \left(a_{reg}^f\right)^*.$$

Then

$$
\left[f_{reg}\frac{df}{d\xi} - f\frac{df_{reg}}{d\xi} + g_{reg}\frac{dg}{d\xi} - g\frac{dg_{reg}}{d\xi} \right]_{-K}^{K} \sim 2ib_{reg}^f(a_{reg}^f + ib_{reg}^f) - 2ia_{reg}^g(-ia_{reg}^g + b_{reg}^g)
$$
$$
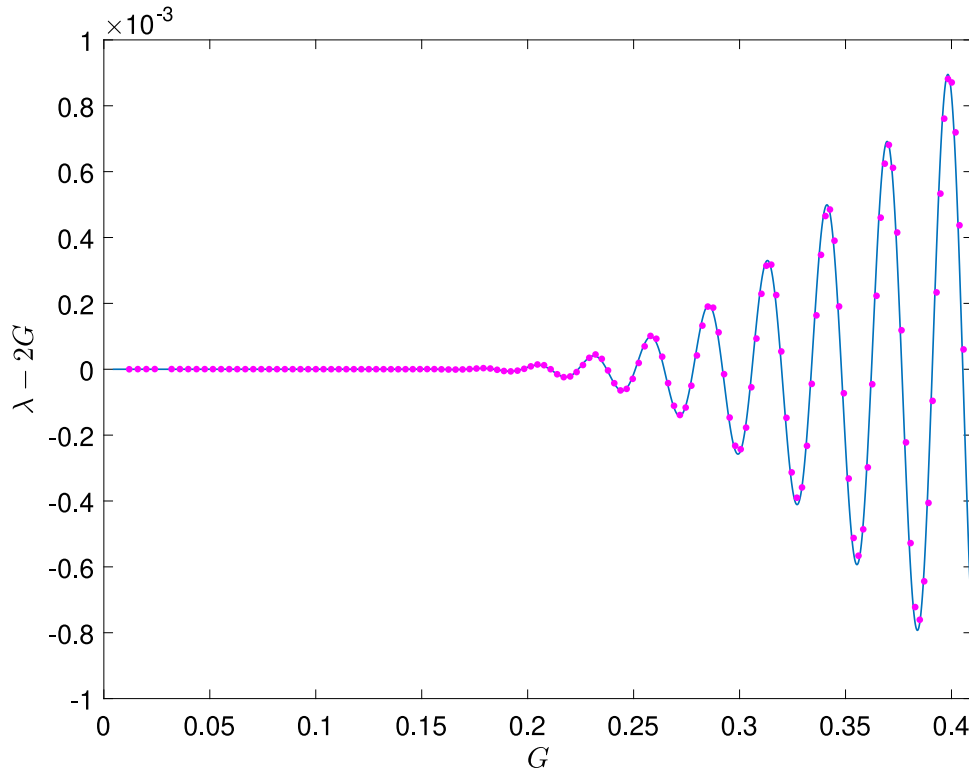\sim -8a_0^2\nu e^{-\pi/G}\mathrm{Re}\left((1 - iG)^2 e^{2i\phi_2(KG)/G}\right),
$$

Fig. 7. Comparison between numerical and the asymptotic predictions, for $K = 20$. The solid blue curve corresponds to Eq. (41), while the purple dots to the numerical solution.

as $\nu \to 0$. Evaluating the right-hand side of Eq. (24) gives

$$i\lambda_{\exp} \int_{-\infty}^{\infty} (g_{\mathrm{reg}}^2 - f_{\mathrm{reg}}^2)\,\mathrm{d}\xi = i\lambda_{\exp} \int_{-\infty}^{\infty} (g_{\mathrm{reg}} - f_{\mathrm{reg}})(g_{\mathrm{reg}} + f_{\mathrm{reg}})\,\mathrm{d}\xi$$

$$= -2G\lambda_{\exp} \int_{-\infty}^{\infty} \left(-2V_s + G^2\xi^2 V_s\right)\left(\frac{V_s}{\sigma} + \xi\frac{\mathrm{d}V_s}{\mathrm{d}\xi}\right)\mathrm{d}\xi$$

$$= -2G\lambda_{\exp} \int_{-\infty}^{\infty} -2V_s^2\left(\frac{1}{\sigma} - \frac{1}{2}\right) + G^2\xi^2 V_s^2\left(\frac{1}{\sigma} - \frac{3}{2}\right)\mathrm{d}\xi,$$

since

$$\int_{-\infty}^{\infty} \xi\frac{\mathrm{d}V_s}{\mathrm{d}\xi}V_s\,\mathrm{d}\xi = -\frac{1}{2}\int_{-\infty}^{\infty} V_s^2\,\mathrm{d}\xi, \qquad \int_{-\infty}^{\infty} \xi^3\frac{\mathrm{d}V_s}{\mathrm{d}\xi}V_s\,\mathrm{d}\xi = -\frac{3}{2}\int_{-\infty}^{\infty} \xi^2 V_s^2\,\mathrm{d}\xi.$$

The dominant contribution to these integrals is from the near field [46]. Using the asymptotic expansion of V_s in powers of G [46] gives

$$\int_{-\infty}^{\infty} V_s^2\,\mathrm{d}\xi = \frac{\sqrt{3}\pi}{2} + \frac{\sqrt{3}\pi^3 G^2}{128} + O(G^4), \qquad \int_{-\infty}^{\infty} \xi^2 V_s^2\,\mathrm{d}\xi = \frac{\sqrt{3}\pi^3}{32} + O(G^2), \tag{40}$$

so that Eq. (24) becomes

$$-8a_0^2\nu e^{-\pi/G}\mathrm{Re}\left((1 - iG)^2 e^{2i\phi_2(KG)/G}\right) = -2\sqrt{3}G\pi\lambda_{\exp}\left(-\left(\frac{1}{\sigma} - \frac{1}{2}\right) + G^2\frac{\pi^2}{32}\left(\frac{1}{\sigma} - \frac{3}{2}\right)\right)$$

$$\sim \frac{\sqrt{3}G^3\pi^3\lambda_{\exp}}{16},$$

since σ is exponentially close to 2. Thus, the correction to the eigenvalue is

$$\lambda_{\exp} \sim -\frac{256\nu e^{-\pi/G}}{G^3\pi^3}\mathrm{Re}\left((1 - iG)^2 e^{2i\phi_2(KG)/G}\right). \tag{41}$$

A comparison between Eq. (41) and the numerically calculated eigenvalue for $K = 20$ is shown in Fig. 7. This shows that our oscillatory correction excellently captures the correction due to the finiteness of the domain around the dominant $\lambda_{\mathrm{reg}} = 2G$.

4.2.2. The eigenvalue $\lambda_{\mathrm{reg}} = G$

In terms of f and g, the approximate eigenfunctions are

$$f_{\mathrm{reg}} = \frac{\mathrm{d}V_s}{\mathrm{d}\xi} - \frac{\mathrm{i}G\xi V_s}{2}, \qquad g_{\mathrm{reg}} = \frac{\mathrm{d}V_s^*}{\mathrm{d}\xi} + \frac{\mathrm{i}G\xi V_s^*}{2}. \tag{42}$$

Again these satisfy the equations exactly, so that $R_{\mathrm{f}} = R_{\mathrm{g}} = 0$, and the perturbation to the eigenvalue arises solely because of the finiteness of the domain.

Comparing Eqs. (42) with Eqs. (30)–(31) as $\rho \to \infty$ gives

$$a_{\mathrm{reg}}^{\mathrm{f}}\left(1 - \mathrm{i}\frac{11G}{48}\right) \sim -\mathrm{i}\sqrt{2}a_0\alpha\left(1 - \mathrm{i}\frac{23G}{48} + \cdots\right), \quad b_{\mathrm{reg}}^{\mathrm{f}}\left(1 + \mathrm{i}\frac{11G}{48}\right) \sim -\mathrm{i}\sqrt{2}a_0\beta\left(1 - \mathrm{i}\frac{G}{48} + \cdots\right),$$

since

$$\mu_1 = \frac{(1 - 12\lambda_1^2)}{48} = -\frac{11}{48}.$$

Thus

$$a_{\mathrm{reg}}^{\mathrm{f}} \sim -\mathrm{i}\sqrt{2}a_0\alpha\left(1 - \frac{\mathrm{i}G}{4}\right), \quad b_{\mathrm{reg}}^{\mathrm{f}} \sim -\mathrm{i}\sqrt{2}a_0\beta\left(1 - \frac{\mathrm{i}G}{4}\right), \quad a_{\mathrm{reg}}^{\mathrm{g}} \sim b_{\mathrm{reg}}^{\mathrm{f}}{}^*, \quad b_{\mathrm{reg}}^{\mathrm{g}} \sim a_{\mathrm{reg}}^{\mathrm{f}}{}^*.$$

Then,

$$\left[f_{\mathrm{reg}}\frac{\mathrm{d}f}{\mathrm{d}\xi} - f\frac{\mathrm{d}f_{\mathrm{reg}}}{\mathrm{d}\xi} + g_{\mathrm{reg}}\frac{\mathrm{d}g}{\mathrm{d}\xi} - g\frac{\mathrm{d}g_{\mathrm{reg}}}{\mathrm{d}\xi}\right]_{-K}^{K} \sim -8a_0^2\nu\mathrm{e}^{-\pi/G}\mathrm{Re}\left((1 - \mathrm{i}G/4)^2\mathrm{e}^{2\mathrm{i}\phi_2(KG)/G}\right).$$

Evaluating the right-hand side of Eq. (24) gives

$$\mathrm{i}\lambda_{\mathrm{exp}}\int_{-\infty}^{\infty}(g_{\mathrm{reg}}^2 - f_{\mathrm{reg}}^2)\,\mathrm{d}\xi = -2G\lambda_{\mathrm{exp}}\int_{-\infty}^{\infty}\xi V_s\frac{\mathrm{d}V_s}{\mathrm{d}\xi}\,\mathrm{d}\xi = G\lambda_{\mathrm{exp}}\int_{-\infty}^{\infty}V_s^2\,\mathrm{d}\xi.$$

Using Eq. (40) gives

$$-8a_0^2\nu\mathrm{e}^{-\pi/G}\mathrm{Re}\left((1 - \mathrm{i}G/4)^2\mathrm{e}^{2\mathrm{i}\phi_2(KG)/G}\right) = G\lambda_{\mathrm{exp}}\frac{\sqrt{3}\pi}{2},$$

i.e.,

$$\lambda_{\mathrm{exp}} \sim -\frac{32\nu\mathrm{e}^{-\pi/G}}{G\pi}\mathrm{Re}\left((1 - \mathrm{i}G/4)^2\mathrm{e}^{2\mathrm{i}\phi_2(KG)/G}\right). \tag{43}$$

In this case, a comparison between Eq. (43) and the numerically calculated eigenvalue for $K = 20$ is shown in Fig. 8. Once again, very good agreement is observed with the numerical finite-domain-induced oscillations, even for values of G that are quite high (i.e., near 0.5).

4.2.3. The eigenvalue $\lambda_{\mathrm{reg}} = -2G$

In terms of f and g the approximate eigenfunctions are

$$f_{\mathrm{reg}} = \mathrm{i}V_s - G\left(\frac{V_s}{\sigma} + \xi\frac{\mathrm{d}V_s}{\mathrm{d}\xi} + \frac{\mathrm{i}G\xi^2 V_s}{2}\right), \quad g_{\mathrm{reg}} = -\mathrm{i}V_s^* - G\left(\frac{V_s^*}{\sigma} + \xi\frac{\mathrm{d}V_s^*}{\mathrm{d}\xi} - \frac{\mathrm{i}G\xi^2 V_s^*}{2}\right). \tag{44}$$

This time, the approximate eigenfunctions do not satisfy the equation exactly, but with an exponentially small residual. We find

$$R_{\mathrm{f}} = -4\mathrm{i}G^2 V_s\left(\frac{1}{2} - \frac{1}{\sigma}\right), \qquad R_{\mathrm{g}} = 4\mathrm{i}G^2 V_s^*\left(\frac{1}{2} - \frac{1}{\sigma}\right),$$

so that

$$\begin{aligned}
\int_{-\infty}^{\infty} R_{\mathrm{f}}f_{\mathrm{reg}} + R_{\mathrm{g}}g_{\mathrm{reg}}\,\mathrm{d}\xi &= 4G^2\left(\frac{1}{2} - \frac{1}{\sigma}\right)\int_{-\infty}^{\infty}\left(2V_s^2 - G^2\xi^2 V_s^2\right)\,\mathrm{d}\xi \\
&= 4G^2\left(\frac{1}{2} - \frac{1}{\sigma}\right)\left(\sqrt{3}\pi + \frac{\sqrt{3}\pi^3 G^2}{64} - \frac{\sqrt{3}\pi^3 G^2}{32} + \cdots\right) \\
&= 4G^2\left(\frac{1}{2} - \frac{1}{\sigma}\right)\left(\sqrt{3}\pi - \frac{\sqrt{3}\pi^3 G^2}{64} + \cdots\right).
\end{aligned}$$

Unfortunately, for $\lambda_{\mathrm{reg}} = -2G$ we will find that we will need to know more than the leading-order behaviour of $a_{\mathrm{reg}}^{\mathrm{f}}$ and $b_{\mathrm{reg}}^{\mathrm{f}}$ in order to find the leading-order approximation to λ_{exp}. Comparing Eqs. (44) with Eqs. (30)–(31) at infinity, including higher-order terms in both expansions (see [46]), gives

$$a_{\mathrm{reg}}^{\mathrm{f}}\left(1 + \mathrm{i}\mu_1 G - \mu_2 G^2 - \mathrm{i}\mu_3 G^3\right) \sim -\mathrm{i}\sqrt{2}a_0\kappa\alpha\left(1 + \frac{\mathrm{i}G}{48} + \frac{2021\mathrm{i}G^3}{1658880} + \cdots\right),$$

$$b_{\mathrm{reg}}^{\mathrm{f}}\left(1 - \mathrm{i}\mu_1 G + \mu_2 G^2 + \mathrm{i}\mu_3 G^3\right) \sim -\mathrm{i}\beta\sqrt{2}a_0\kappa\left(1 + \mathrm{i}\frac{95G}{48} - \frac{17G^2}{24} + \frac{23899\mathrm{i}G^3}{1658880} + \cdots\right),$$
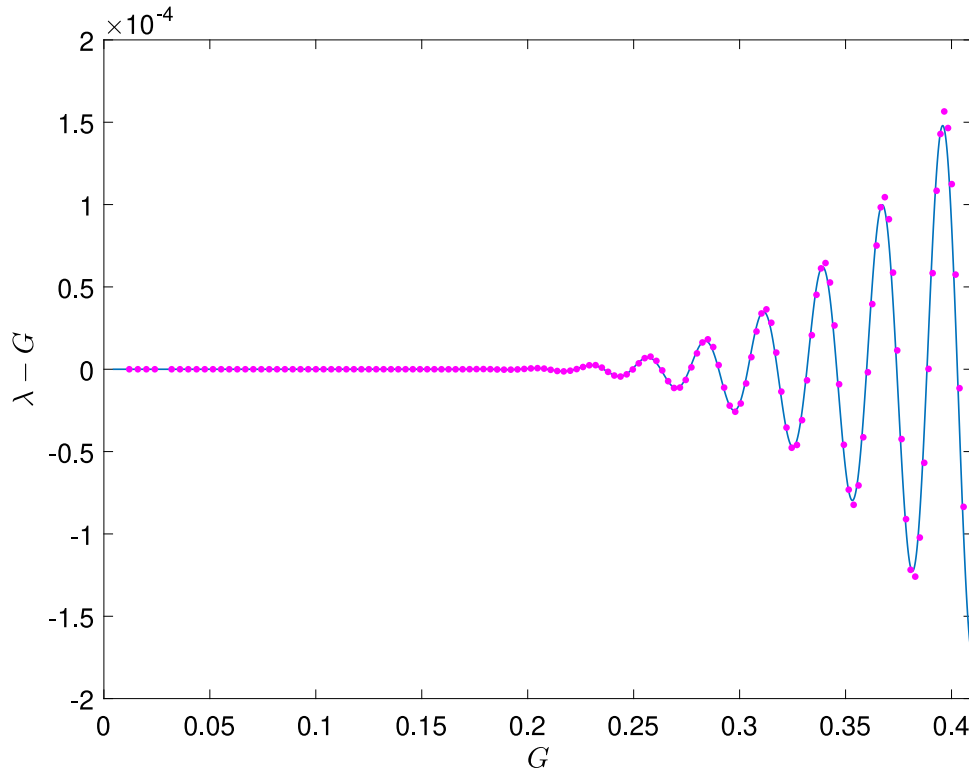
Fig. 8. Comparison between numerical and the asymptotic predictions, for $K = 20$. The solid blue curve corresponds to Eq. (43), while the purple dots pertain to numerical solution.

where

$$\kappa \sim 1 - \left(\frac{1 + 12\pi^2}{4608}\right) G^2 + 0.0152 G^4 + \cdots.$$

Since

$$\mu_1 = \frac{(1 - 12\lambda_1^2)}{48} = -\frac{47}{48}, \quad \mu_2 = \frac{\lambda_1(1 - 4\lambda_1^2)}{48} = \frac{5}{8}, \quad \mu_3 = -\frac{450581}{1658880},$$

we find

$$a_{\text{reg}}^{\text{f}} \sim -i\alpha\sqrt{2}a_0\kappa \left(1 + iG - \frac{17G^2}{48} + \frac{iG^3}{128} + \cdots\right),$$

$$b_{\text{reg}}^{\text{f}} \sim -i\beta\sqrt{2}a_0\kappa \left(1 + iG - \frac{17G^2}{48} + \frac{iG^3}{128} + \cdots\right)$$

as well as

$$a_{\text{reg}}^{\text{g}} = \left(b_{\text{reg}}^{\text{f}}\right)^*, \qquad b_{\text{reg}}^{\text{g}} = \left(a_{\text{reg}}^{\text{f}}\right)^*.$$

Then, as $KG \to \infty$,

$$\left[f_{\text{reg}}\frac{df}{d\xi} - f\frac{df_{\text{reg}}}{d\xi} + g_{\text{reg}}\frac{dg}{d\xi} - g\frac{dg_{\text{reg}}}{d\xi}\right]_{-K}^{K}$$

$$\sim -2ia_{\text{reg}}^{\text{f}}(-ia_{\text{reg}}^{\text{f}})\left(1 - (i\mu_1 G - \mu_2 G^2 + \cdots)^2\right) + 2ib_{\text{reg}}^{\text{g}}(ib_{\text{reg}}^{\text{g}})\left(1 - (-i\mu_1 G - \mu_2 G^2 + \cdots)^2\right)$$

$$\sim 8\sqrt{3}ie^{-\pi/G}\kappa^2 \left(1 + iG - \frac{17G^2}{48} + \frac{iG^3}{128} + \cdots\right)^2 \left(1 - (i\mu_1 G - \mu_2 G^2 + \cdots)^2\right)$$

$$- 8\sqrt{3}ie^{-\pi/G}\kappa^2 \left(1 - iG - \frac{17G^2}{48} - \frac{iG^3}{128} + \cdots\right)^2 \left(1 - (-i\mu_1 G - \mu_2 G^2 + \cdots)^2\right)$$

$$\sim -32\sqrt{3}\, e^{-\pi/G}\kappa^2 \left(G + \frac{G^3}{2304} + \cdots\right).$$
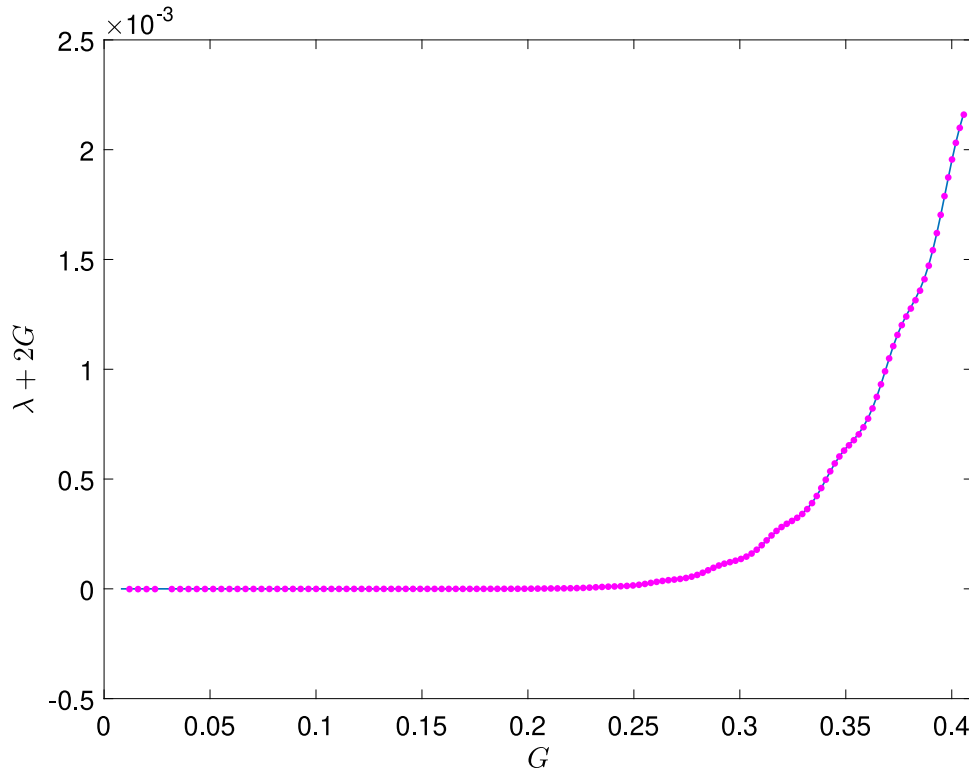
Fig. 9. Asymptotic prediction (46) (blue) compared to numerical solution (purple) for the case of the eigenvalue with $\lambda_{\text{reg}} = -2G$.

Evaluating the right-hand side of Eq. (24) gives

$$i\lambda_{\exp} \int_{-\infty}^{\infty} (g_{\text{reg}}^2 - f_{\text{reg}}^2)\,d\xi = 2G\lambda_{\exp} \int_{-\infty}^{\infty} \left(-2V_s + G^2\xi^2 V_s\right)\left(\frac{V_s}{\sigma} + \xi\frac{dV_s}{d\xi}\right) d\xi$$

$$= 2G\lambda_{\exp} \int_{-\infty}^{\infty} -2V_s^2\left(\frac{1}{\sigma} - \frac{1}{2}\right) + G^2\xi^2 V_s^2\left(\frac{1}{\sigma} - \frac{3}{2}\right) d\xi,$$

after integrating by parts. Using (40) we find that (24) becomes

$$-32\sqrt{3}\,e^{-\pi/G}\kappa^2 G\left(1 + \frac{G^2}{2304} + \cdots\right) + 4G^2\left(\frac{1}{2} - \frac{1}{\sigma}\right)\left(\sqrt{3}\pi - \frac{\sqrt{3}\pi^3 G^2}{64}\right)$$

$$= 2\sqrt{3}G\pi\lambda_{\exp}\left(-\left(\frac{1}{\sigma} - \frac{1}{2}\right) + G^2\frac{\pi^2}{32}\left(\frac{1}{\sigma} - \frac{3}{2}\right)\right)$$

$$\sim -\frac{2\sqrt{3}G^3\pi^3\lambda_{\exp}}{32}. \tag{45}$$

Now, since (for $\nu \sim 0$) the relation between σ and G is (see [46])

$$G\left(\frac{1}{2} - \frac{1}{\sigma}\right)\left(\frac{\sqrt{3}\pi}{4} + \frac{\sqrt{3}\pi^3 G^2}{256} + \cdots\right) = 2\sqrt{3}\kappa^2 e^{-\pi/G},$$

we find the leading terms on the left-hand side of (45) vanish. This is the reason we needed to include the higher-order corrections; these give the correction to the eigenvalue as

$$\lambda_{\exp} \sim G\left(1 - \frac{2}{\sigma}\right)\left(1 + \frac{1}{72\pi^2}\right) + \cdots. \tag{46}$$

A comparison between (46) and the numerically calculated eigenvalue for $K = 20$ is shown in Fig. 9. Note that although we derived (46) in the limit $K \to \infty$, $\nu \to 0$, when we plot it in Fig. 9 we use the finite-domain approximation to σ as a function of G. We can see that for this eigenvalue we do not purely observe the oscillatory effect induced by the finite nature of the domain as in the two previous cases. Rather, the relevant correction incorporates also the deviation from the exact scaling symmetry (and hence from the symmetry of the eigenvalue pair at $\pm 2G$) which provides the monotonic portion of the relevant correction.

4.2.4. The eigenvalue $\lambda_{\mathrm{reg}} = -G$

In terms of f and g, the approximate eigenfunctions are

$$f_{\mathrm{reg}} = \frac{dV_s}{d\xi} + \frac{iG\xi V_s}{2}, \qquad g_{\mathrm{reg}} = \frac{dV_s^*}{d\xi} - \frac{iG\xi V_s^*}{2}. \tag{47}$$

These satisfy the equations exactly, so that $R_{\mathrm{f}} = R_{\mathrm{g}} = 0$. However, they do not satisfy the correct radiation condition at infinity. In the finite domain context, the perturbation of the eigenvalue arises from the boundary terms in Eq. (24).

Comparing Eq. (47) with Eqs. (30)–(31) as $\rho \to \infty$ gives

$$a_{\mathrm{reg}}^{\mathrm{f}}\left(1 - i\frac{11G}{48}\right) \sim i\sqrt{2}a_0\alpha\left(1 + i\frac{G}{48} + \cdots\right), \quad b_{\mathrm{reg}}^{\mathrm{f}}\left(1 + i\frac{11G}{48}\right) \sim i\sqrt{2}a_0\beta\left(1 + i\frac{23G}{48} + \cdots\right),$$

since

$$\mu_1 = \frac{(1 - 12\lambda_1^2)}{48} = -\frac{11}{48}.$$

Thus,

$$a_{\mathrm{reg}}^{\mathrm{f}} \sim i\sqrt{2}a_0\alpha\left(1 + \frac{iG}{4}\right), \quad b_{\mathrm{reg}}^{\mathrm{f}} \sim i\sqrt{2}a_0\beta\left(1 + \frac{iG}{4}\right), \quad a_{\mathrm{reg}}^{\mathrm{g}} \sim \left(b_{\mathrm{reg}}^{\mathrm{f}}\right)^*, \quad b_{\mathrm{reg}}^{\mathrm{g}} \sim \left(a_{\mathrm{reg}}^{\mathrm{f}}\right)^*.$$

When $\lambda_1 = -1$, $S \to e^{2i\phi_2/G}$ as $\nu \to 0$, so we need to use the full expressions

$$a_{\mathrm{f}} \sim -\frac{b_{\mathrm{reg}}^{\mathrm{f}} + a_{\mathrm{reg}}^{\mathrm{f}}S}{i + S}, \qquad b_{\mathrm{f}} \sim -i\frac{b_{\mathrm{reg}}^{\mathrm{f}} + a_{\mathrm{reg}}^{\mathrm{f}}S}{i + S}, \tag{48}$$

for a_{f} and b_{f}. Then

$$\left[f_{\mathrm{reg}}\frac{df}{d\xi} - f\frac{df_{\mathrm{reg}}}{d\xi} + g_{\mathrm{reg}}\frac{dg}{d\xi} - g\frac{dg_{\mathrm{reg}}}{d\xi}\right]_{-K}^{K} \sim \mathrm{Re}\left(-4i(a_{\mathrm{reg}}^{\mathrm{f}}b_{\mathrm{f}} - b_{\mathrm{reg}}^{\mathrm{f}}a_{\mathrm{f}})\left(1 + \mu_1^2G^2 + \cdots\right)\right)$$

$$\sim \mathrm{Re}\left(-\frac{8ia_0^2(1 + iG/4)^2}{i + S}(i\alpha - \beta)(S\alpha + \beta)\left(1 + \mu_1^2G^2 + \cdots\right)\right)$$

$$\sim \mathrm{Re}\left(\frac{8ia_0^2(1 + iG/4)^2}{i + S}Se^{-\pi/G}\left(1 + \mu_1^2G^2 + \cdots\right)\right)$$

$$\sim \mathrm{Re}\left(\frac{16i\sqrt{3}(1 + iG/4)^2}{1 + ie^{-2i\phi_2/G}}e^{-\pi/G}\right).$$

Since the integrals in Eq. (23) are dominated by the near field, where V_s is real, using the near-field solution in Eq. (23) gives

$$i\lambda_{\exp}\int_{-\infty}^{\infty}(g_{\mathrm{reg}}^2 - f_{\mathrm{reg}}^2)\,d\xi = i\lambda_{\exp}\int_{-\infty}^{\infty}(g_{\mathrm{reg}} - f_{\mathrm{reg}})(g_{\mathrm{reg}} + f_{\mathrm{reg}})\,d\xi$$

$$= 2G\lambda_{\exp}\int_{-\infty}^{\infty}\xi V_s\frac{dV_s}{d\xi}\,d\xi$$

$$= -G\lambda_{\exp}\int_{-\infty}^{\infty}V_s^2\,d\xi \sim -G\lambda_{\exp}\frac{\sqrt{3}\pi}{2}.$$

Thus the correction to the eigenvalue is

$$\lambda_{\exp} \sim -\mathrm{Re}\left(\frac{32i(1 + iG/4)^2}{\pi G(1 + ie^{-2i\phi_2/G})}e^{-\pi/G}\right). \tag{49}$$

A comparison between Eq. (49) and the numerically calculated eigenvalue for $K = 20$ is shown in Fig. 10. A key feature to observe here is the presence of vertical asymptotes in this exponentially small (in G) correction. These represent the reason for the jumps observed in Fig. 10. Indeed, it is relevant to note that a particularly careful observation of the orange line in Fig. 6 will reveal the outcome of these jumps to the particularly astute reader, as can be discerned, e.g., near the outermost disconnect of the relevant numerical line. Despite the fact that our theoretical approximation can no longer be considered accurate when $\lambda_{\exp}$ becomes large, we can still see that it very accurately captures our numerical results of Fig. 10.

We see from the numerical results that there is a very thin transition region in the vicinity of each asymptote in which the eigenvalue perturbation switches from large and positive to large and negative. We do not attempt to capture this transition region, which requires a detailed calculation in the vicinity of $S = -i$.

4.2.5. The eigenvalues near $\lambda = 0$

In terms of f and g the approximate eigenfunctions are

$$f_{\mathrm{reg}} = iV_s, \qquad g_{\mathrm{reg}} = -iV_s^*. \tag{50}$$

In fact, these satisfy the equations and boundary conditions exactly, so that $\lambda = 0$ is an exact eigenvalue even for a finite domain. However, as we have seen numerically, there is a second eigenvalue which is exponentially close to zero, which we now approximate. This analysis does not fit into the general framework of Section 4, but follows a similar methodology, which we now outline.
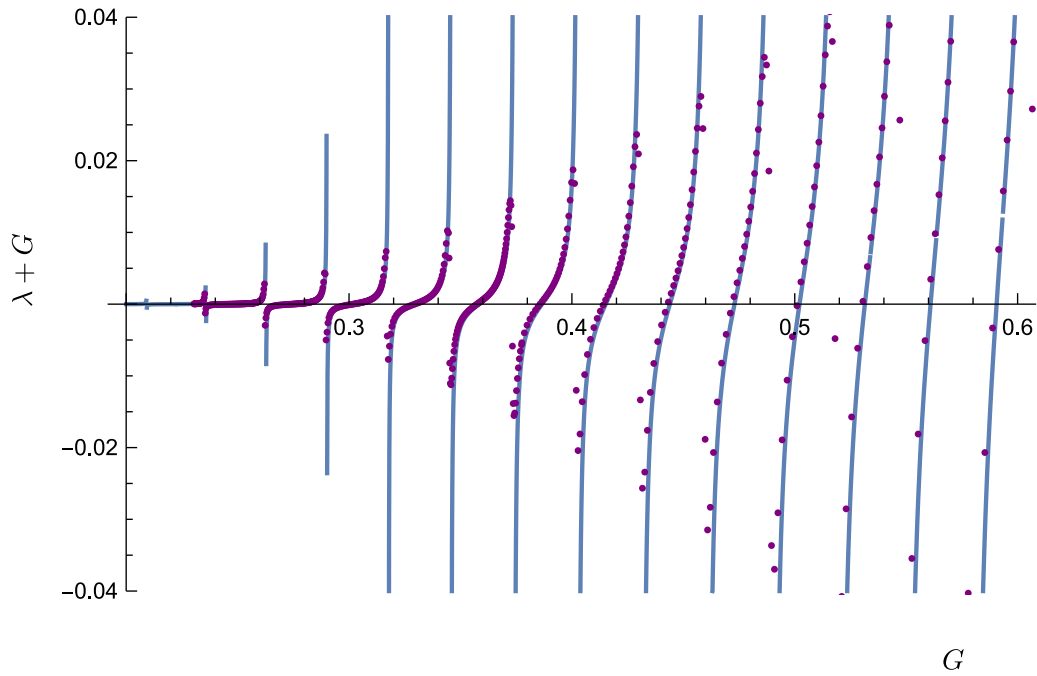
Fig. 10. Asymptotic prediction [cf. Eq. (49)] (blue) compared to numerical solution (purple), for the eigenvalues with $\lambda_{\text{reg}} = -G$ and for $K = 20$.

We write

$$f = iV_s + \lambda_{\exp_1} f_1 + f_{\exp}, \tag{51}$$

$$g = -iV_s^* + \lambda_{\exp_1} g_1 + g_{\exp}, \tag{52}$$

$$\lambda = \lambda_{\exp_1} + \lambda_{\exp_2}, \tag{53}$$

where $\lambda_{\exp_2} \ll \lambda_{\exp_1}$ and

$$\frac{d^2 f_1}{d\xi^2} + \sigma |V_s|^{2\sigma-2}(V_s^*)^2 g_1 + (\sigma+1)|V_s|^{2\sigma} f_1 - f_1 - \frac{i(\sigma-2)G}{2\sigma} f_1 + \frac{G^2 \xi^2}{4} f_1 = V_s^*, \tag{54}$$

$$\frac{d^2 g_1}{d\xi^2} + \sigma |V_s|^{2\sigma-2}(V_s)^2 f_1 + (\sigma+1)|V_s|^{2\sigma} g_1 - g_1 + \frac{i(\sigma-2)G}{2\sigma} g_1 + \frac{G^2 \xi^2}{4} g_1 = V_s, \tag{55}$$

with

$$\frac{df_1}{d\xi} = \frac{iG\xi f_1}{2}, \qquad \frac{dg_1}{d\xi} = -\frac{iG\xi g_1}{2} \qquad \text{at } \xi = K.$$

Note that the linear operator here is slightly different from (but exponentially close to) that of Eqs. (19)–(20), and is chosen so that the solvability condition is exactly satisfied, so that we can be sure that f_1, g_1 exist: multiplying Eq. (54) by V_s and Eq. (55) by $-V_s^*$ adding and integrating gives

$$\int_{-K}^{K} \left(\frac{d^2 f_1}{d\xi^2} + \sigma |V_s|^{2\sigma-2}(V_s^*)^2 g_1 + (\sigma+1)|V_s|^{2\sigma} f_1 - f_1 - \frac{i(\sigma-2)G}{2\sigma} f_1 + \frac{G^2 \xi^2}{4} f_1 \right) V_s \, d\xi$$

$$- \int_{-K}^{K} \left(\frac{d^2 g_1}{d\xi^2} + \sigma |V_s|^{2\sigma-2} V_s^2 f_1 + (\sigma+1)|V_s|^{2\sigma} g_1 - g_1 + \frac{i(\sigma-2)G}{2\sigma} g_1 + \frac{G^2 \xi^2}{4} g_1 \right) V_s^* \, d\xi$$

$$= \int_{-K}^{K} \left(\frac{d^2 V_s}{d\xi^2} + |V_s|^{2\sigma} V_s - V_s - \frac{i(\sigma-2)G}{2\sigma} V_s + \frac{G^2 \xi^2}{4} V_s \right) f_1 \, d\xi$$

$$- \int_{-K}^{K} \left(\frac{d^2 V_s^*}{d\xi^2} + |V_s|^{2\sigma} V_s^* - V_s^* + \frac{i(\sigma-2)G}{2\sigma} V_s^* + \frac{G^2 \xi^2}{4} V_s^* \right) g_1 \, d\xi$$

$$+ \left[V_s \frac{df_1}{d\xi} - f_1 \frac{dV_s}{d\xi} - V_s^* \frac{dg_1}{d\xi} + g_1 \frac{dV_s^*}{d\xi} \right]_{-K}^{K}$$

$$= \left[V_s \frac{iG\xi f_1}{2} - f_1 \frac{iG\xi V_s}{2} - V_s^* \frac{(-iG\xi g_1)}{2} + g_1 \frac{(-iG\xi V_s^*)}{2} \right]_{-K}^{K} = 0.$$

Now, substituting Eqs. (51)–(53) into Eqs. (19)–(20) gives

$$\frac{d^2 f_{\exp}}{d\xi^2} + \sigma |V_s|^{2\sigma-2} V_s^2 g_{\exp} + (\sigma+1)|V_s|^{2\sigma} f_{\exp} - f_{\exp} - \frac{i(\sigma-2)G}{2\sigma} f_{\exp} + \frac{G^2 \xi^2}{4} f_{\exp}$$

$$= \lambda_{\exp_1} \sigma |V_s|^{2\sigma-2}((V_s^*)^2 - V_s^2) g_1 + \lambda_{\exp_1}(V_s - V_s^*) - i\lambda_{\exp_1}^2 f_1 + \lambda_{\exp_2} V_s,$$

$$\frac{d^2 g_{\exp}}{d\xi^2} + \sigma |V_s|^{2\sigma-2}(V_s^*)^2 f_{\exp} + (\sigma+1)|V_s|^{2\sigma} g_{\exp} - g_{\exp} + \frac{i(\sigma-2)G}{2\sigma} g_{\exp} + \frac{G^2 \xi^2}{4} g_{\exp}$$

$$= \lambda_{\exp_1} \sigma |V_s|^{2\sigma-2}(V_s^2 - (V_s^*)^2) f_1 + \lambda_{\exp_1}(V_s^* - V_s) + i\lambda_{\exp_1}^2 g_1 + \lambda_{\exp_2} V_s^*,$$

where we have neglected triply-exponentially-small terms involving $\lambda_{\exp_2} \lambda_{\exp_1}$. Multiplying by iV_s, $-iV_s^*$, adding and integrating the LHS is triply exponentially small. After simplifying, and neglecting the triply-exponentially-small term $(V_s^2 - (V_s^*)^2)\lambda_{\exp_2}$, the RHS gives

$$\int_{-\infty}^{\infty} i\lambda_{\exp_1} \sigma |V_s|^{2\sigma-2}((V_s^*)^2 - V_s^2)(V_s g_1 + V_s^* f_1) + i\lambda_{\exp_1}(V_s^2 - (V_s^*)^2) + \lambda_{\exp_1}^2(V_s f_1 + V_s^* g_1)\, d\xi \sim 0. \tag{56}$$

This is the equation which will determine the eigenvalue $\lambda_{\exp_1}$; note that it is quadratic, and $\lambda_{\exp_1} = 0$ is a solution as expected. In the outer region f_1 and g_1 are exponentially small. Thus the integrals involving f_1 and g_1 are dominated by the inner region. In the inner region $f_1 = g_1 +$ exponentially small terms, and

$$\frac{d^2 f_1}{d\xi^2} + 5V_s^4 f_1 - f_1 + \frac{G^2 \xi^2}{4} f_1 = V_s.$$

We find

$$f_1 = \frac{1}{2}\left(\frac{V_s}{2} + \xi \frac{dV_s}{d\xi}\right) + G^2 f_{12},$$

where, up to exponentially small terms,

$$\frac{d^2 f_{12}}{d\xi^2} + 5V_s^4 f_{12} - f_{12} + \frac{G^2 \xi^2}{4} f_{12} = \frac{1}{2}\xi^2 V_s.$$

Unfortunately we need to find this correction term f_{12} because the leading-order term will integrate to zero. Expanding in powers of G, we find $f_{12} \sim -2V_1$ where $V_s \sim V_0 + G^2 V_1 + \cdots$ (see [46]), so that

$$\int_{-\infty}^{\infty} (V_s f_1 + V_s^* g_1)\, d\xi \sim \int_{-\infty}^{\infty} V_s \left(\frac{V_s}{2} + \xi \frac{dV_s}{d\xi} - 4G^2 V_1\right) d\xi \sim -4G^2 \int_{-\infty}^{\infty} V_0 V_1\, d\xi = -\frac{G^2 \sqrt{3}\pi^3}{64}.$$

The dominant contribution to the integral of $(V_s^2 - (V_s^*)^2)$ comes from the outer region before the turning point, in which, with $\xi = \rho/G$,

$$V_s \sim \frac{2^{1/2} a_0}{(4 - \rho^2)^{1/4}}(e^{\phi(\rho)/G} + \gamma e^{-\phi(\rho)/G}), \qquad \phi = -\int_0^\rho \left(1 - \frac{\bar\rho^2}{4}\right)^{1/2} d\bar\rho, \qquad \gamma = \frac{i e^{-\pi/G}}{2},$$

(see [46]), so that

$$i\int_{\infty}^{\infty}(V_s^2 - (V_s^*)^2)\, d\xi \sim \frac{2i}{G}\int_0^2 (V_s + V_s^*)(V_s - V_s^*)\, d\rho \sim \frac{2i}{G}\int_0^2 2\frac{2^{1/2} a_0 e^{\phi(\rho)/G}}{(4 - \rho^2)^{1/4}} 2\frac{2^{1/2} a_0 \gamma e^{-\phi(\rho)/G}}{(4 - \rho^2)^{1/4}}\, d\rho$$

$$\sim -\frac{16\sqrt{3} e^{-\pi/G}}{G}\int_0^2 \frac{d\rho}{(4 - \rho^2)^{1/2}} = -\frac{8\sqrt{3}\pi\, e^{-\pi/G}}{G}.$$

The final term in Eq. (56) is subdominant, so that, to leading order, Eq. (56) gives

$$\lambda_{\exp_1} = -\frac{8\sqrt{3}\pi e^{-\pi/G}}{G}\frac{64}{G^2\sqrt{3}\pi^3} = -\frac{512\, e^{-\pi/G}}{G^3 \pi^2}. \tag{57}$$

In Appendix D, we show that the asymptotic behaviour (57) can be determined much more simply from the reduced system derived in [46], which describes the slow evolution of G in the vicinity of the bifurcation.

Fig. 11 shows the asymptotic prediction Eq. (57) against a direct numerical simulation. For this eigenvalue the convergence is slower as $G \to 0$ so that the leading-order approximation is not as close to the numerical solution. This is because the higher-order corrections are significant when estimating the integrals in Eq. (56). To demonstrate this we also show in Fig. 11 the approximation

$$\lambda_{\exp_1} \sim -i\frac{\int_{-\infty}^{\infty}(V_s - (V_s^*)^2)\, d\xi}{\int_{-\infty}^{\infty}(V_s f_1 - V_s^* g_1)\, d\xi} \tag{58}$$

with a numerical solution for V_s, f_1 and g_1, which converges more quickly to the numerical value. It is clear that the latter expression of Eq. (58) captures the dependence on G more accurately than the leading-order correction of the former.

4.3. Continuous spectrum

Finally we consider the problem of identifying the continuous spectrum asymptotically as $G \to 0$. In the far field with $\rho = G\xi$, neglecting the exponentially small terms $|V_s|^{2\sigma}$ and $(\sigma - 2)$, we have

$$i\lambda f + G^2 \frac{d^2 f}{d\rho^2} - f + \frac{\rho^2}{4}f = 0, \qquad -i\lambda g + G^2 \frac{d^2 g}{d\rho^2} - g + \frac{\rho^2}{4}g = 0, \tag{59}$$
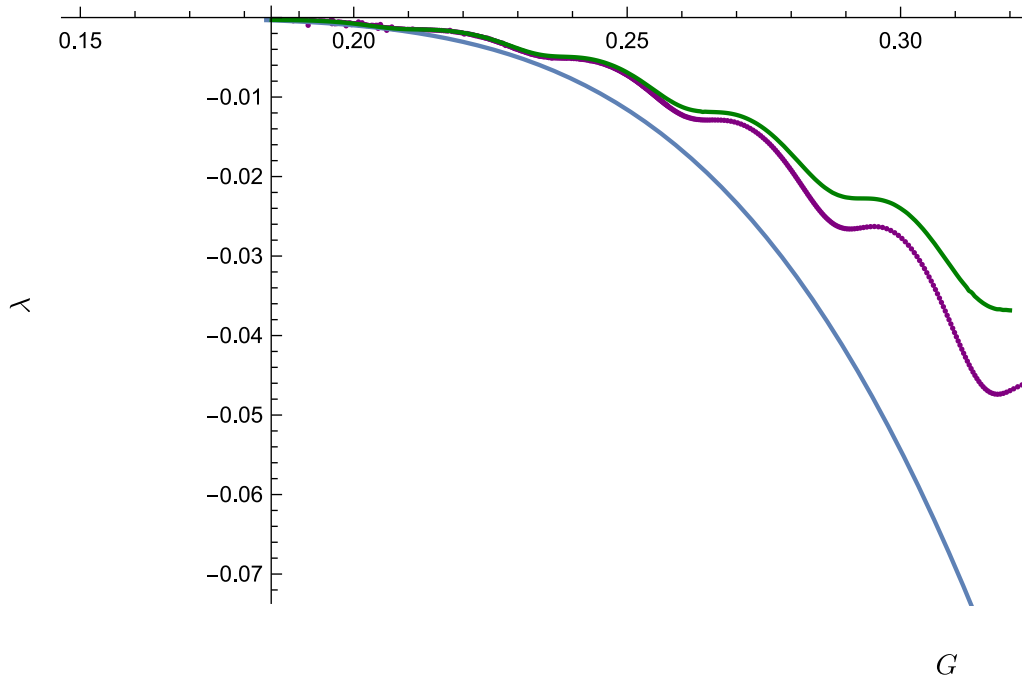
Fig. 11. Asymptotic prediction [cf. Eq. (57)] (blue) compared to numerical solution (purple), for the eigenvalue in the vicinity of $\lambda_{reg} = 0$, for $K = 20$. Also shown (green) is the approximation (58).

along with the boundary conditions

$$G\frac{df}{d\rho} = \frac{i\rho f}{2}, \qquad G\frac{dg}{d\rho} = -\frac{i\rho g}{2} \qquad \text{at } \rho = \pm KG.$$

Let us start by imagining that these equations hold throughout the region $[-KG, KG]$, before returning to investigate the impact of the inner region near $\rho = 0$.

Since the equations for f and g decouple (because we have ignored the inner region), we can treat them separately, and each will give a set of eigenvalues. In fact, we see that for any eigenfunction–eigenvalue pair (f, λ) the conjugates (f^*, λ^*) satisfy the equations and boundary conditions for g. We therefore start by focusing on the equation for f.

Using the WKB expansion

$$f = A_f e^{i\phi_f/G} + B_f e^{-i\phi_f/G},\tag{60}$$

where

$$A_f = \sum_{n=0}^{\infty} A_{fn}(\rho)(iG)^n, \qquad B_f = \sum_{n=0}^{\infty} B_{fn}(\rho)(-iG)^n,$$

$$i\lambda - (\phi_f')^2 - 1 + \frac{\rho^2}{4} = 0,$$

$$2i\phi_f' A_{f0}' + i\phi_f'' A_{f0} = 0, \qquad -2i\phi_f' B_{f0}' - i\phi_f'' B_{f0} = 0,$$

we find

$$\phi_f = \int_0^\rho \left(\frac{\bar{\rho}^2}{4} - 1 + i\lambda\right)^{1/2} d\bar{\rho} = \frac{\rho}{4}\sqrt{\rho^2 - 4 + 4i\lambda} + (-1 + i\lambda)\log\left(\frac{\rho + \sqrt{\rho^2 - 4 + 4i\lambda}}{\sqrt{-4 + 4i\lambda}}\right),$$

with

$$A_{f0} = a_f\left(\frac{\rho^2}{4} - 1 + i\lambda\right)^{-1/4}, \qquad B_{f0} = b_f\left(\frac{\rho^2}{4} - 1 + i\lambda\right)^{-1/4}.$$

Note that this expansion differs from that performed previously in that we have included λ at leading order rather than assuming that $\lambda = O(G)$.

There are two turning points, at

$$\rho = \rho_{f\pm} = \pm 2(1 - i\lambda)^{1/2}.$$

In order to define uniquely ϕ_f let us put branch cuts from these turning points to $\pm i\infty$ away from the real axis, as indicated in Fig. 12 for an arbitrary but representative value of λ.
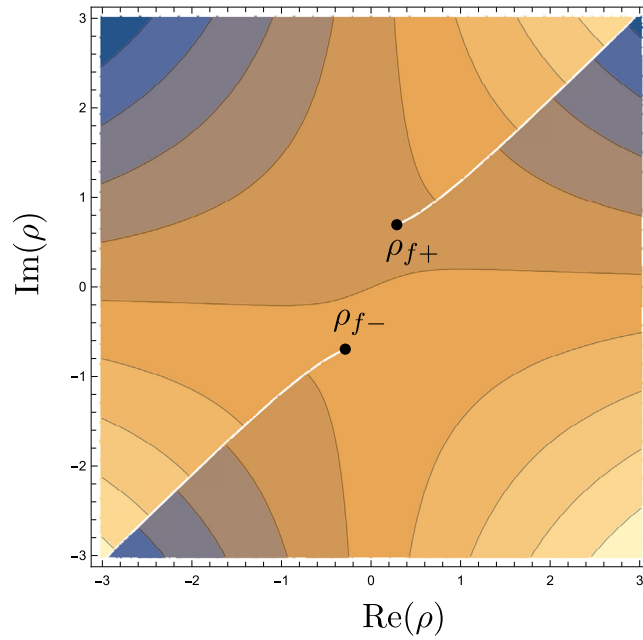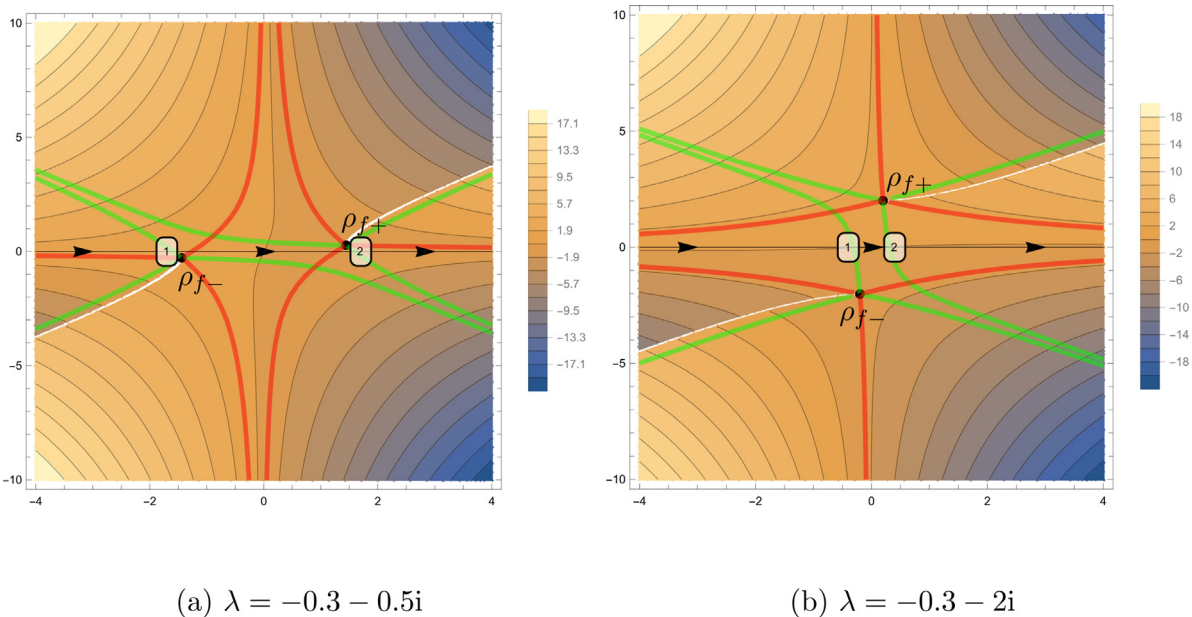
Fig. 12. Branch points and branch cuts in ϕ_f when $\lambda = -0.1 - 1.1i$. The contour shading corresponds to $\text{Im}(\phi_f)$.

(a) $\lambda = -0.3 - 0.5i$

(b) $\lambda = -0.3 - 2i$

Fig. 13. Stokes lines (green) and anti-Stokes lines (red). The contour shading corresponds to $\text{Im}(\phi_f)$. The path along the real axis is indicated, as well as the two points at which Stokes lines are crossed.

To impose the boundary conditions on Eq. (60) we need to take account of the change in the coefficients a_f and b_f due to Stokes phenomenon (see e.g. [49,50]). In Fig. 13 we illustrate the Stokes lines associated with each of the turning points for various values of λ. Let us calculate the change in the coefficients a_f and b_f as we cross Stokes lines when moving from $\rho = -KG$ to $\rho = KG$. We suppose that $\text{Re}(\lambda) < 0$ so that ρ_+ is in the first quadrant. Although the topology of the anti-Stokes lines changes as $\text{Im}(\lambda)$ varies, as we move along the real axis from minus infinity to infinity we always cross one Stokes line from each turning point. Across these Stokes lines the dominant WKB approximation will turn on a multiple of the subdominant WKB approximation.

The first Stokes line we cross, indicated by a "1" in Fig. 13, is that which moves up from ρ_{f-}, on which $\text{Im}(\phi_f(\rho)) > \text{Im}(\phi_f(\rho_{f-}))$. Thus $e^{-i\phi_f/G}$ is the exponentially dominant term, and the coefficient a_f changes by $-ib_f e^{-2i\phi_f(\rho_{f-})/G}$. The second Stokes line we cross, indicated by a "2" in Fig. 13, is that which moves down from ρ_{f+}, on which $\text{Im}(\phi_f(\rho)) < \text{Im}(\phi_f(\rho_{f+}))$. This on this Stokes line $e^{i\phi_f/G}$ is the exponentially dominant term, and the coefficient b_f changes by $ia_f e^{2i\phi_f(\rho_{f+})/G}$. Thus, together, the change in the coefficient is

$$
(a_f^{-\infty}, b_f^{-\infty}) \rightarrow (a_f^{-\infty} - ib_f^{-\infty}e^{-2i\phi_f(\rho_{f-})/G}, b_f^{-\infty})
$$
$$
\rightarrow (a_f^{-\infty} - ib_f^{-\infty}e^{-2i\phi_f(\rho_{f-})/G}, b_f^{-\infty} + i(a_f^{-\infty} - ib_f^{-\infty}e^{-2i\phi_f(\rho_{f-})/G})e^{2i\phi_f(\rho_{f+})/G}),
$$

so that

$$a_f^\infty = a_f^{-\infty} - ib_f^{-\infty}e^{-2i\phi_f(\rho_{f-})/G},$$
$$b_f^\infty = b_f^{-\infty} + ia_f^{-\infty}e^{2i\phi_f(\rho_{f+})/G} + b_f^{-\infty}e^{-2i\phi_f(\rho_{f-})/G}e^{2i\phi_f(\rho_{f+})/G}.$$

The boundary condition at $\rho = KG$ gives, at leading order,

$$e^{2i\phi_f(KG)/G}\frac{\sqrt{(KG)^2 - 4 + 4i\lambda} - KG}{\sqrt{(KG)^2 - 4 + 4i\lambda} + KG} = \frac{B_{f0}(KG)}{A_{f0}(KG)} = \frac{b_f^\infty}{a_f^\infty}.$$

The boundary condition at $\rho = -KG$ gives, at leading order,

$$e^{2i\phi_f(-KG)/G}\frac{\sqrt{(KG)^2 - 4 + 4i\lambda} + KG}{\sqrt{(KG)^2 - 4 + 4i\lambda} - KG} = \frac{B_{f0}(-KG)}{A_{f0}(-KG)} = \frac{b_f^{-\infty}}{a_f^{-\infty}}.$$

Noting that ϕ_f is odd, if we let

$$Q_f = e^{2i\phi_f(KG)/G}\frac{\sqrt{(KG)^2 - 4 + 4i\lambda} - KG}{\sqrt{(KG)^2 - 4 + 4i\lambda} + KG}, \tag{61}$$

then we have the following homogeneous system of four equations in the four unknowns $a_f^\infty, b_f^\infty, a_f^{-\infty}, b_f^{-\infty}$,

$$b_f^\infty = Q_f a_f^\infty,$$
$$a_f^{-\infty} = Q_f b_f^{-\infty},$$
$$a_f^\infty = a_f^{-\infty} - ib_f^{-\infty}e^{-2i\phi_f(\rho_{f-})/G},$$
$$b_f^\infty = b_f^{-\infty} + ia_f^{-\infty}e^{2i\phi_f(\rho_{f+})/G} + b_f^{-\infty}e^{-2i\phi_f(\rho_{f-})/G}e^{2i\phi_f(\rho_{f+})/G}.$$

Noting that $\phi_f(\rho_{f+}) = -\phi_f(\rho_{f-}) = -(\lambda + i)\pi/2$, the condition for a non-trivial solution is

$$(Q_f - ie^{(1-i\lambda)\pi/G})^2 = 1. \tag{62}$$

For finite K, Eq. (62) gives a discrete set of eigenvalues with the separation between neighbouring eigenvalues becoming smaller as $K \to \infty$, approximating the continuous spectrum. For large K,

$$Q_f \sim e^{iK^2G/2}e^{-i(1+i\lambda)/G}(-1 + i\lambda)^{1+(i+\lambda)/G}(KG)^{-2-2(i+\lambda)/G}.$$

For $\text{Im}(\lambda) < 0$ we need $|Q_f| \sim 1$ as $G \to 0$ to get a balance in Eq. (62), which requires $\text{Re}(\lambda) \sim -G$. For $\text{Im}(\lambda) > 0$ we need $Q_f \sim ie^{(1-i\lambda)\pi/G}$ as $G \to 0$ to get a balance in Eq. (62), which also requires $\text{Re}(\lambda) \sim -G$. Thus the continuous spectrum of the problem [cf. Eq. (59)] lies close to (but not exactly on) the line $\text{Re}(\lambda) = -G$. The calculation for g is similar and gives the same equation as Eq. (62) with $\lambda \to \lambda^*$ as expected. In Fig. 14 we compare the predictions of Eq. (62) (recalling the definition of Eq. (61)) with the numerical evaluation of the eigenvalues of Eq. (59). A very good agreement is found between the latter (identified as black dots) and the former (identified via the intersection of the contours of the blue and red curves associated with the real and the imaginary parts of Eq. (62)).

We now consider how the picture above changes when we include the inner region. Then, in addition to the Stokes lines already considered, there is a change in the coefficients a and b as we pass from $\rho = 0-$ to $\rho = 0+$. The connection formula comes from matching the solution in the inner region with the far field expansions on each side. Note that f and g are coupled in the inner region, so that we no longer have two separate eigenvalue problems. Specifically, at leading order in the inner region V_s is real and

$$i\lambda f + \frac{d^2f}{d\xi^2} + 2V_s^4g + 3V_s^4f - f = 0, \tag{63}$$

$$-i\lambda g + \frac{d^2g}{d\xi^2} + 2V_s^4f + 3V_s^4g - g = 0, \tag{64}$$

with

$$f \sim a_f^{0+}\frac{e^{i\phi_f(0)/G}}{(-1 + i\lambda)^{1/4}}e^{(1-i\lambda)^{1/2}\xi} + b_f^{0+}\frac{e^{i\phi_f(0)/G}}{(-1 + i\lambda)^{1/4}}e^{-(1-i\lambda)^{1/2}\xi} \quad \text{as } \xi \to \infty,$$

$$g \sim a_g^{0+}\frac{e^{i\phi_g(0)/G}}{(-1 - i\lambda)^{1/4}}e^{-(1+i\lambda)^{1/2}\xi} + b_g^{0+}\frac{e^{i\phi_g(0)/G}}{(-1 - i\lambda)^{1/4}}e^{(1+i\lambda)^{1/2}\xi} \quad \text{as } \xi \to \infty,$$

$$f \sim a_f^{0-}\frac{e^{i\phi_f(0)/G}}{(-1 + i\lambda)^{1/4}}e^{(1-i\lambda)^{1/2}\xi} + b_f^{0-}\frac{e^{i\phi_f(0)/G}}{(-1 + i\lambda)^{1/4}}e^{-(1-i\lambda)^{1/2}\xi} \quad \text{as } \xi \to -\infty,$$

$$g \sim a_g^{0-}\frac{e^{i\phi_g(0)/G}}{(-1 - i\lambda)^{1/4}}e^{-(1+i\lambda)^{1/2}\xi} + b_g^{0-}\frac{e^{i\phi_g(0)/G}}{(-1 - i\lambda)^{1/4}}e^{(1+i\lambda)^{1/2}\xi} \quad \text{as } \xi \to -\infty.$$

The solution gives connection formulae between the incoming coefficients $a_f^{0-}, b_f^{0-}, a_g^{0-}$ and b_g^{0-} and the outgoing coefficients $a_f^{0+}, b_f^{0+}, a_g^{0+}$ and b_g^{0+}. Unfortunately it is not possible to determine these formulae analytically.

However, when λ is large the first two terms in Eqs. (63) and (64) dominate, and the solution is of WKB form even in the inner region. The phase factor is trivial, with no turning points, so that there is no change in coefficient. Thus for large λ the eigenvalues should be well approximated by Eq. (62).
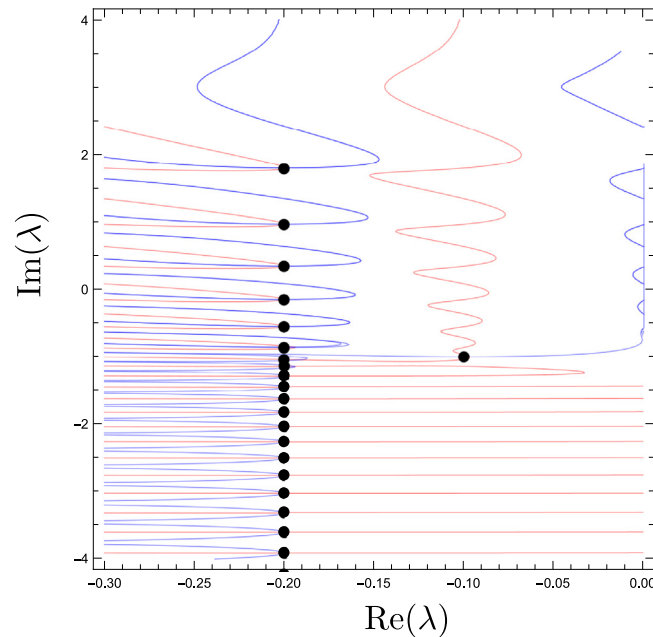
Fig. 14. Eigenvalues for the problem of Eq. (59) for f (black points), for $G = 0.2$. The contours show the asymptotic prediction of Eq. (62). The red curves correspond to $\mathrm{Im}(Q_f - \mathrm{i}e^{(1-\mathrm{i}\lambda)\pi/G}) = 0$, while the blue curves correspond to $\mathrm{Re}(Q_f - \mathrm{i}e^{(1-\mathrm{i}\lambda)\pi/G}) \in \{-1, 1\}$. The eigenvalues should lie at the intersections of these contours. The approximation is very good, apart from near $\lambda = -\mathrm{i}$, at which point the two turning points $\rho_{f\pm} = \pm 2(1 - \mathrm{i}\lambda)^{1/2}$ coalesce.

On the other hand when $\lambda = 0$ we find by solving Eqs. (63)–(64) as a power series in G that

$$a_f^{0+} \sim a_g^{0-}, \quad b_f^{0+} \sim -b_g^{0-}, \quad b_g^{0+} \sim b_f^{0-}, \quad a_g^{0+} \sim -a_f^{0-},$$

so that there must be some mixing of the coefficients in f and g for small λ. Identifying the details of the relevant spectrum at small λ remains a challenging question for future study.

5. Conclusions & future challenges

In the present work, we have revisited the topic of stability of solutions that are self-similarly blowing up. We followed up on the earlier work of [45] with substantially improved numerical means and techniques, and also added a systematic theoretical understanding, building also on important works in the intermediate time interval (such as the key contributions of [43,44]). This has allowed us to obtain a systematic understanding of the 3 eigenvalue pairs of the Hamiltonian system at the critical point of $\sigma d = 2$ and its continuous spectrum. We advocated the relevance of exploring the self-similar solutions in the co-exploding frame, by analogy with the study of travelling solutions in a co-travelling frame, as per the standard dynamical systems perspective [41,42]. We have also explained systematically why, despite the presence of positive real eigenvalues, the relevant self-similar solution is not genuinely unstable but only subject to effectively neutral eigendirections. To corroborate the relevant results, we performed direct numerical simulations in the renormalized frame, verifying (in line with earlier computations) the attractivity of the relevant waveforms.

Naturally, this analysis raises a number of interesting questions for further research. Understanding the dynamics (and the potential role of self-similarity) slightly below the critical point $\sigma d = 2$ is an example of this type. Moreover, we have argued that the supercritical solutions considered herein are effectively stable, upon explaining the origin of their real eigendirections. Yet, it is well-known that there are other problems for which multiple, higher-order collapsing solutions branches exist, some among which are dynamically unstable: a notable example of this sort is, e.g., the complex Ginzburg–Landau equation [51]. It is then of particular interest to explore such waveforms via the type of spectral analysis proposed herein, and corroborate in a systematic fashion their stability or instability, as well as leverage such spectral information in an attempt to understand the corresponding direct numerical simulations of the relevant system in the renormalized frame. In a different vein, there are other important dispersive PDE models that feature similar bifurcations towards the emergence of collapsing solutions, such as the generalized KdV problem; for a recent exposition of the collapsing solutions and asymptotics thereof, see, e.g., [40]. It is then of particular interest to adapt the methodology proposed herein to the latter problem to explore the potential generality of the eigenvalue phenomenology identified in the present work. Such topics are presently under active investigation and relevant results will be reported in future publications.

CRediT authorship contribution statement

S.J. Chapman: Conceptualization, Data curation, Formal analysis, Investigation, Methodology, Validation, Visualization, Writing – original draft. **M. Kavousanakis:** Data curation, Investigation, Methodology, Software, Validation, Visualization, Writing – original draft. **E.G. Charalampidis:** Investigation, Software, Validation, Visualization, Writing – review & editing. **I.G. Kevrekidis:** Conceptualization, Investigation, Methodology, Writing – review & editing. **P.G. Kevrekidis:** Conceptualization, Formal analysis, Funding acquisition, Investigation, Methodology, Project administration, Writing – original draft.

Declaration of competing interest

Acknowledgements

Appendix A. An instructive ODE example

Consider, arguably, one of the simplest self-similar problems, namely the ODE:

$$\dot{x} = x^p, \quad x(t) \in \mathbb{R}. \tag{A.1}$$

In order to leverage the self-similar frame to analyse this problem, we seek to absorb the temporal dependence through a transformation to go to a frame where the solution appears steady. In this (ODE) case, it is not a steady spatial profile, as in the PDE example studied throughout this work, but instead a "number". We thus use $x(t) = A(\tau)\bar{x}$ with $\tau = \tau(t)$ corresponding to a rescaling of time (to be determined), and obtain the steady-state problem $\bar{x} = \bar{x}^p$ leading to $\bar{x} = 0$ or $\bar{x} = 1$. Then, in accordance to general self-similarity principles [52,53], we select

$$\frac{A_\tau}{A} = 1 \Rightarrow A = A_0 e^\tau; \quad \tau_t = A^{p-1} \Rightarrow A(t) = \left[\frac{1}{(p-1)(t^\star - t)}\right]^{\frac{1}{p-1}} = A_0 \left[\frac{1}{(t^\star - t)}\right]^{\frac{1}{p-1}}. \tag{A.2}$$

In Eq. (A.2), $t^\star$ denotes the blow-up time, i.e., $x(t) \to \infty$ as $t \nearrow t^\star$. In the self-similar frame, we have indeed devised a much more elaborate way to obtain a simple ODE result. The innate advantage of the method, however, is that in this frame that "explodes" with the solution it is possible to perform a stability analysis using:

$$x(t) = A(\tau)[\bar{x} + \epsilon y(\tau)] \Rightarrow y_\tau = (p-1)y, \quad \epsilon \ll 1, \tag{A.3}$$

assuming that we keep the leading order ($O(\epsilon)$) terms in y. We thus observe that the self-similar frame features a single eigenvalue (indeed, since it is an ODE rather than a PDE) of $\lambda = p - 1$. For collapsing solutions with $p > 1$, this is an eigenvalue associated with growth since $\lambda > 0$.

A natural question then is whether this is a *true* instability. The perturbation $A(\tau)\epsilon y$ can be rewritten as $\epsilon e^{p\tau} \sim \epsilon(t^\star - t)^{p/(1-p)}$. But then, considering a shift in the collapse time $t^\star \to t^\star + \tilde{\epsilon}\delta t$ ($\tilde{\epsilon} \ll 1$), and substituting it in the original solution, we obtain:

$$x(t) \to \widetilde{x}(t) = \left[\frac{1}{p-1}\right]^{\frac{1}{p-1}} \left[\frac{1}{t^\star + \tilde{\epsilon}\delta t - t}\right]^{\frac{1}{p-1}} = A_0 \left[\frac{1}{t^\star - t}\right]^{\frac{1}{p-1}} - \left(\frac{\tilde{\epsilon}A_0\delta t}{p-1}\right)(t^\star - t)^{\frac{p}{1-p}}. \tag{A.4}$$

Namely, the positive eigenvalue does *not* correspond to a true instability but rather is associated with the translational invariance of the ODE with respect to the shifting of the collapse time.

Appendix B. Continuous spectra obtained from the rescaled NLS equation

Fig. B.1 depicts numerical spectra of the rescaled NLS equation obtained for different σ values. One can observe the alignment of eigenvalues on a nearly vertical line of continuous spectrum, with real part, $\lambda_r = -G$. As we move away from the critical value, $\sigma = 2$, the distortions from the vertical line become progressively larger.

Appendix C. Effect of size domain on the numerical computations

Fig. C.1 presents a comparison of the computed spectra of the rescaled NLS equation for size domain $K = 20$ and $K = 40$. Even by doubling the size of the computational domain, the alignment of eigenvalues on a "vertical" line of the continuous spectrum remains practically unchanged (although slightly closer to the line $\text{Re}(\lambda) = -G$), and the real eigenvalues deviations are also visually indistinguishable.

Appendix D. Stability of the reduced system

In [46], asymptotic solutions of Eq. (12) were constructed which result in the following reduced system for the growth rate G and an associated variable β, which can be thought of as the normal form associated with the bifurcation:

$$\frac{dG}{d\tau} = \beta - G^2, \tag{D.1}$$

$$c_0 \frac{d\beta}{d\tau} = \frac{(\sigma - 2)}{2\sigma} b_0 G - A_1^2 \text{sign}(G) e^{-\pi/|G|}, \tag{D.2}$$

where A_1, c_0 and b_0 are given by (10). This is a slow-fast system with fast Eq. (D.1) and slow Eq. (D.2); Eq. (9) corresponds to the quasistatic approximation $\beta = G^2$.
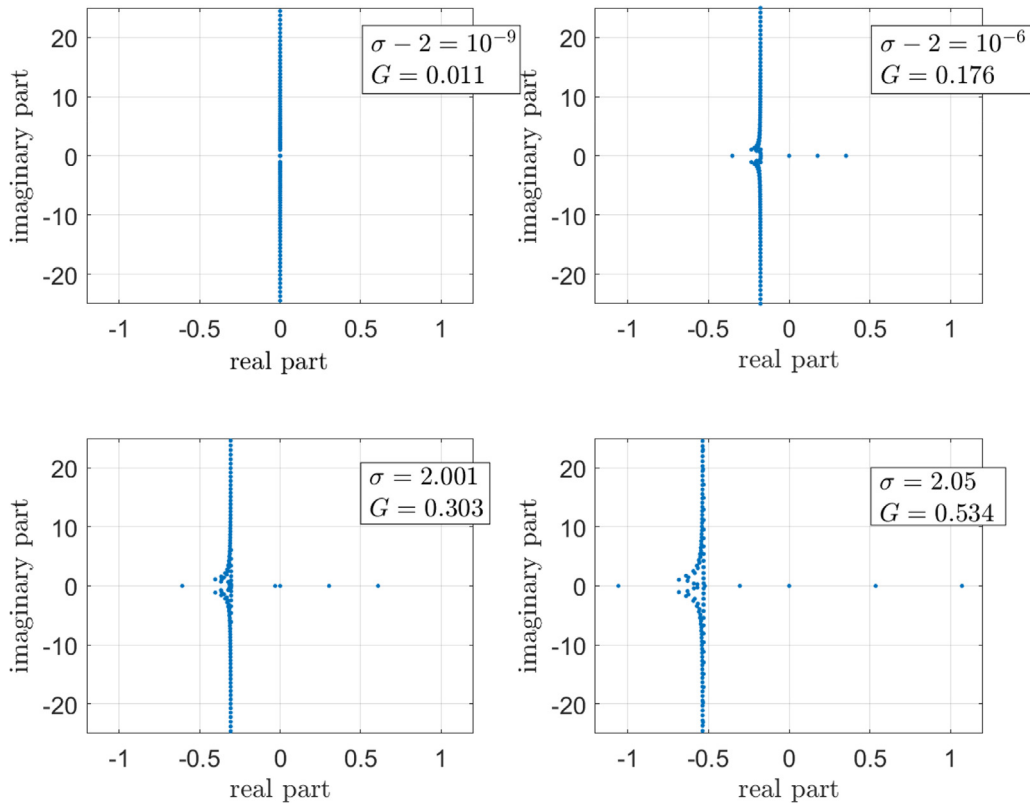
Fig. B.1. Continuous spectra obtained from the numerical solution of the rescaled NLS equation with $K = 20$ and σ values close to the critical value, $\sigma = 2$: $\sigma = 2 + 10^{-9}$ (top left panel) and $\sigma = 2 + 10^{-6}$ (top right panel), as well as $\sigma = 2.001$ (bottom left panel), $\sigma = 2.05$ (bottom right panel).
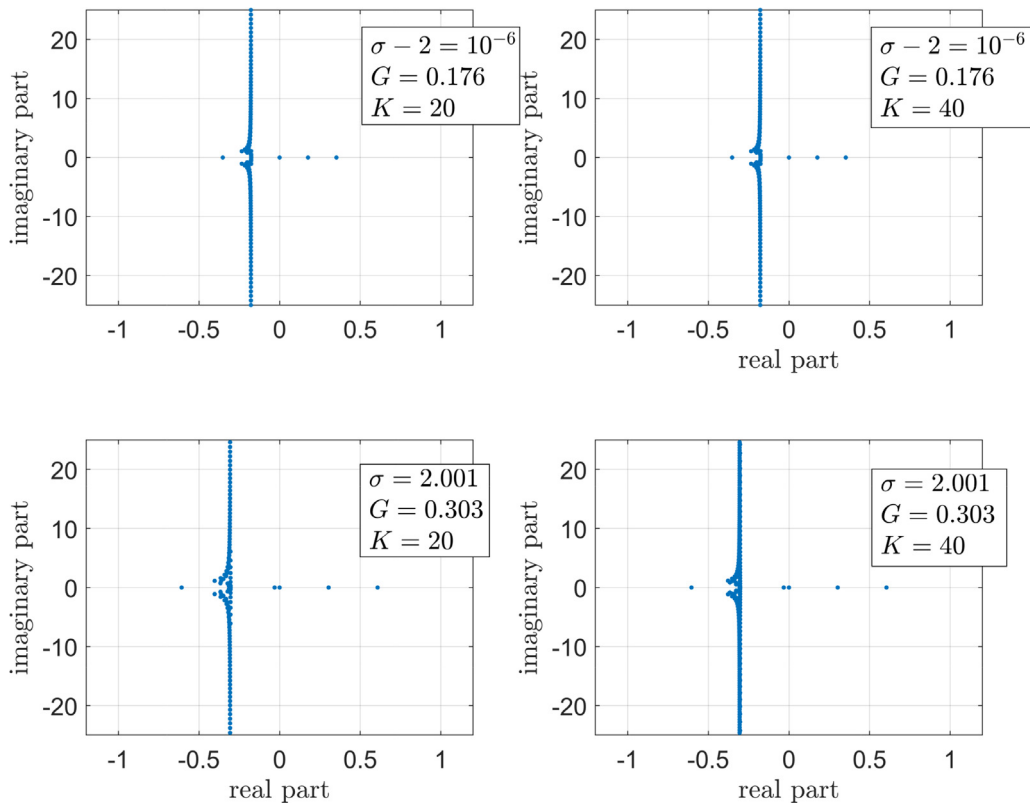
Fig. C.1. Comparison of spectra obtained from the numerical solution of the rescaled NLS equation for size domain $K = 20$ (left panel) and $K = 40$ (right panel).

D.1. Stability of the zero solution

Linearizing about the origin gives

$$\frac{dG}{d\tau} = \beta,$$
$$\frac{d\beta}{d\tau} = \frac{(\sigma - 2)b_0}{2\sigma c_0}G.$$

The characteristic equation is

$$\lambda^2 = \frac{(\sigma - 2)b_0}{2\sigma c_0},$$

showing a pair of eigenvalues moving from the imaginary axis to the real axis as σ passes through 2 as expected.

D.2. Stability of the non-zero solution

The steady solution (G_0, β_0) given by

$$\beta_0 = G_0^2, \qquad \frac{(\sigma - 2)}{2\sigma}b_0 G_0 = A_1^2 e^{-\pi/G_0}.$$

with $G_0 > 0$ corresponds to the blow-up solution in the original frame. Perturbing about this solution by writing $G = G_0 + x$, $\beta = G_0^2 + y$ and linearizing gives

$$\frac{dx}{d\tau} = y - 2G_0 x,$$
$$c_0 \frac{dy}{d\tau} = \frac{(\sigma - 2)}{2\sigma}b_0 x - A_1^2 e^{-\pi/G_0}\frac{\pi}{G_0^2}x.$$

The characteristic equation is

$$\lambda(\lambda + 2G_0) - \frac{1}{c_0}\left(\frac{(\sigma - 2)}{2\sigma}b_0 - A_1^2 e^{-\pi/G_0}\frac{\pi}{G_0^2}\right) = 0.$$

One eigenvalue is exponentially close to zero, while one is exponentially close to $-2G_0$. The exponentially small eigenvalue is approximately

$$\lambda \sim \frac{1}{2c_0 G_0}\left(\frac{(\sigma - 2)}{2\sigma}b_0 - A_1^2 e^{-\pi/G_0}\frac{\pi}{G_0^2}\right) \sim -A_1^2 e^{-\pi/G_0}\frac{\pi}{2c_0 G_0^3} \sim -\frac{e^{-\pi/G_0}}{512 G_0^3 \pi^2},$$

in agreement with the detailed calculation of Section 4.2.5. Note that this is also the eigenvalue which remains when reducing Eqs. (D.1)–(D.2) to the slow manifold giving

$$2c_0 G \frac{dG}{d\tau} = \frac{(\sigma - 2)}{2\sigma}b_0 G - A_1^2 \operatorname{sign}(G)e^{-\pi/|G|}. \tag{D.3}$$

We note that the exponentially small correction to the eigenvalue $\lambda \sim -2G$ does not agree with the detailed calculation in Section 4.2.3. This is due to the fact that it corresponds to an exponentially small correction of the fast timescale, and the system of Eqs. (D.1)–(D.2) is accurate at leading-order only in that regime.

References

[1] M.J. Ablowitz, H. Segur, Solitons and the Inverse Scattering Transform, SIAM, Philadelphia, 1981.
[2] M.J. Ablowitz, P.A. Clarkson, Solitons, Nonlinear Evolution Equations and Inverse Scattering, Cambridge University Press, Cambridge, 1991.
[3] M.J. Ablowitz, B. Prinari, A.D. Trubatch, Discrete and Continuous Nonlinear Schrödinger Systems, Cambridge University Press, Cambridge, 2004.
[4] C. Sulem, P.L. Sulem, The Nonlinear Schrödinger Equation, Springer-Verlag, New York, 1999.
[5] P.G. Kevrekidis, D.J. Frantzeskakis, R. Carretero-González, The Defocusing Nonlinear Schrödinger Equation: From Dark Solitons and Vortices to Vortex Rings, SIAM, Philadelphia, 2015.
[6] A. Hasegawa, Solitons in Optical Communications, Clarendon Press, Oxford, NY, 1995.
[7] Yu.S. Kivshar, G.P. Agrawal, Optical Solitons: From Fibers to Photonic Crystals, Academic Press, San Diego, 2003.
[8] M. Kono, M.M. Skorić, Nonlinear Physics of Plasmas, Springer-Verlag, Heidelberg, 2010.
[9] E. Infeld, G. Rowlands, Nonlinear Waves, Solitons and Chaos, Cambridge University Press, Cambridge, 1990.
[10] M.J. Ablowitz, Nonlinear Dispersive Waves: Asymptotic Analysis and Solitons, Cambridge University Press, Cambridge, 2011.
[11] L.P. Pitaevskii, S. Stringari, Bose–Einstein Condensation, Oxford University Press, Oxford, 2003.
[12] C.J. Pethick, H. Smith, Bose–Einstein Condensation in Dilute Gases, Cambridge University Press, Cambridge, 2002.
[13] G. Fibich, The Nonlinear Schrödinger Equation, Singular Solutions and Optical Collapse, Springer-Verlag, New York, 2015.
[14] F.Kh. Abdullaev, A. Gammal, A.M. Kamchatnov, L. Tomio, Internat. J. Modern Phys. B 19 (2005) 3415.
[15] D.J. Frantzeskakis, J. Phys. A (2010).
[16] R.W. Boyd, S.G. Lukishova, Y.R. Shen, Self-Focusing: Past and Present, Springer-Verlag, New York, 2009.
[17] G. Fibich, G. Papanicolaou, SIAM J. Appl. Math. 60 (1999) 183.
[18] L. Bergé, Phys. Rep. 303 (1998) 259.
[19] Yu.S. Kivshar, D.E. Pelinovsky, Phys. Rep. 331 (2000) 117.
[20] P.M. Lushnikov, S.A. Dyachenko, N. Vladimirova, Phys. Rev. A 88 (2013) 013845.
[21] P.M. Lushnikov, N. Vladimirova, Opt. Express 23 (2015) 31120.
[22] B. Shim, S.E. Schrauth, A.L. Gaeta, M. Klein, G. Fibich, Phys. Rev. Lett. 108 (2012) 043902.

[23] H. Koch, Nonlinearity 28 (2015) 545.
[24] K. Yang, S. Roudenko, Y. Zhao, Nonlinearity 31 (2018) 4354.
[25] K.D. Moll, A.L. Gaeta, G. Fibich, Phys. Rev. Lett. 90 (2003) 203902.
[26] L.T. Vuong, T.D. Grow, A. Ishaaya, A.L. Gaeta, G.W. 't Hooft, E.R. Eliel, G. Fibich, Phys. Rev. Lett. 96 (2006) 133901.
[27] A. Sagiv, A. Ditkowski, G. Fibich, Opt. Express 25 (2017) 24387.
[28] M. Centurion, M.A. Porter, P.G. Kevrekidis, D. Psaltis, Phys. Rev. Lett. 97 (2006) 033903.
[29] C.-A. Chen, C.-L. Hung, Phys. Rev. Lett. 127 (2021) 060404.
[30] B. Bakkali-Hassani, C. Maury, Y.-Q. Zou, É. Le Cerf, R. Saint-Jalm, P.C.M. Castilho, S. Nascimbene, J. Dalibard, J. Beugnon, Phys. Rev. Lett. 127 (2021) 023603.
[31] E.A. Donley, N.R. Claussen, S.L. Cornish, J.L. Roberts, E.A. Cornell, C.E. Wieman, Nature 412 (2001) 295.
[32] S.L. Cornish, S.T. Thompson, C.E. Wieman, Phys. Rev. Lett. 96 (2006) 170401.
[33] A. Di Carli, C.D. Colquhoun, G. Henderson, S. Flannigan, G.-L. Oppo, A.J. Daley, S. Kuhr, E. Haller, Excitation modes of bright matter-wave solitons, Phys. Rev. Lett. 123 (2019) 123602.
[34] D. Luo, Y. Jin, J.H.V. Nguyen, B.A. Malomed, O.V. Marchukov, V.A. Yurovsky, V. Dunjko, M. Olshanii, R.G. Hulet, Creation and characterization of matter-wave breathers, Phys. Rev. Lett. 125 (2020) 183902.
[35] V.A. Galaktionov, E.L. Mitidieri, S.I. Pohozaev, Blow-Up for Higher-Order Parabolic, Hyperbolic, Dispersion and Schrödinger Equations, CRC Press, Boca Raton, 2014.
[36] W. Ren, X.-P. Wang, J. Comput. Phys. 159 (2000) 246–273.
[37] C.J. Budd, V. Rottschaeffer, J.F. Williams, SIAM J. Appl. Dyn. Syst. 4 (2005) 649–678.
[38] C.J. Budd, J.F. Williams, J. Engrg. Math. 66 (2010) 217–236.
[39] V.A. Galaktionov, Stud. Appl. Math. 124 (2010) 347–381.
[40] P. Amodio, C.J. Budd, O. Koch, V. Rottschäfer, G. Settanni, E. Weinmüller, Physica D 401 (2020) 132179.
[41] B. Sandstede, Stability of travelling waves, in: B. Fiedler (Ed.), Handbook of Dynamical Systems, 2002, p. 983.
[42] T. Kapitula, K. Promislow, Spectral and Dynamical Stability of Nonlinear Waves, Springer-Verlag, New York, 2013.
[43] A.J. Bernoff, T.P. Witelski, Appl. Math. Lett. 15 (2002) 599–606.
[44] A.J. Bernoff, T.P. Witelski, J. Engrg. Math. 66 (2010) 11–31.
[45] C.I. Siettos, I.G. Kevrekidis, P.G. Kevrekidis, Nonlinearity 16 (2003) 497–506.
[46] S.J. Chapman, M. Kavousanakis, I.G. Kevrekidis, P.G. Kevrekidis, Phys. Rev. E 104 (2021) 044202.
[47] D.J. Kaup, Phys. Rev. A 42 (1990) 5689.
[48] J. Kestyn, E. Polizzi, P.T.P. Tang, SIAM J. Sci. Comput. 38 (2016) S772.
[49] H.J.W. Müller-Kirsten, Introduction to Quantum Mechanics: Schrödinger Equation and Path Integral, World Scientific, 2012.
[50] S.J. Chapman, J. Fluid Mech. 451 (2002) 35–97.
[51] C.J. Budd, V. Rottschäfer, J.F. Williams, SIAM J. Appl. Dyn. Syst. 4 (2005) 649.
[52] G.I. Barenblatt, Scaling, Self-Similarity and Intermediate Asymptotics, Cambridge University Press, Cambridge, 1996.
[53] W. Huang, R.D. Russell, Adaptive Moving Mesh Methods, Springer-Verlag, New York, 2010.